Int J Earth Sci (Geol Rundsch) (2012) 101:973–996
DOI 10.1007/s00531-011-0699-2

ORIGINAL PAPER

Pressure–temperature evolution of eclogites from the Kechros complex in the Eastern Rhodope (NE Greece)

E. Mposkos · I. Baziotis · A. Proyer

Received: 13 February 2011 / Accepted: 8 July 2011 / Published online: 2 August 2011
© Springer-Verlag 2011

Abstract The Rhodope Domain in NE Greece consists of different tectonometamorphic complexes involved in the Alpine collisional history between the Eurasian and African plates. In the Kechros Complex, which is the lowermost tectonic unit in the East Rhodope, a lense of kyanite eclogite occurs within orthogneiss and common eclogites are found between serpentinized peridotite and underlying pelitic gneisses. In kyanite eclogite, the high-pressure (HP) mineral assemblage is Grt + Omp ($Jd_{35–55}$) + Ky + Ph + Qz + Rt + (indirectly inferred Tlc + Law); a Na-rich tremolite and zoisite formed at or near peak metamorphic conditions. In common eclogites, the HP mineral assemblage is Grt + Omp (Jd29–41) + Rt and, with less certainty, Amp (Gln-rich + Brs + Wnc + Hbl) ± Czo. The inclusions in garnet are glaucophane, actinolite, barroisite, hornblende, omphacite, clinozoisite, titanite, rutile and rarely paragonite and albite. In kyanite eclogite, peak *P–T* conditions are constrained at 2.2 GPa and 615°C using garnet–omphacite–phengite geothermobarometry and very similar values of 585 ± 32°C and 2.17 ± 0.11 GPa with the average *P–T* method, by which conditions of formation could also be narrowed down for the common eclogite (619 ± 53°C and 1.69 ± 0.17 GPa) and for a retrogressed eclogite (534 ± 36°C and 0.77 ± 0.11 GPa). Ages for the HP metamorphism in the Kechros Complex are not yet available. A Rb–Sr white mica age of 37 Ma from orthogneiss records a stage of the exhumation. The HP event may be coeval with the Eocene HP metamorphism (49–55 Ma) recorded in the Nestos Shear Zone in Central Rhodope and in the Attic-Cycladic crystalline belt, where it is interpreted as the result of subduction and final closure of the Axios/Vardar ocean and subsequent subduction of the Apulian continental crust (a promontory of the Africa continent) under the southern margin of the European continent in the late Cretaceous and early Tertiary.

Keywords Kyanite eclogites · Common eclogites · Rhodope · HP metamorphism · Thermobarometry · Pseudosection

E. Mposkos (✉) · I. Baziotis
Department of Mining and Metallurgical Engineering, Section of Geological Sciences, National Technical University of Athens, Heroon Polytechniou 9, 15780 Athens, Greece
e-mail: mposkos@metal.ntua.gr

I. Baziotis
e-mail: baziotis@metal.ntua.gr

A. Proyer
Institute of Earth Sciences, Mineralogy and Petrology, Karl-Franzens University, Universitätsplatz 2/II, 8010 Graz, Austria
e-mail: alexander.proyer@uni-graz.at

Introduction

Detailed petrological analyses of high-P metamorphic areas provide direct information on deep-seated tectonic processes that occurred along fossil subduction zones and on the history of convergent plate margins. This is important as such processes are not accessible to direct observation at active convergent plate margins. Eclogites are very important for the investigation into subducted plates because they preserve the PT record of subduction much better than gneisses and metapelites. The Rhodope Domain provides the opportunity for studying the complex tectonic history of a convergent plate margin during subduction and subsequent continental collision.

The Rhodope Domain (RD, including the Rhodope and Serbomacedonian Zone s.s.) was previously considered as

a craton surrounded by two branches of the Alpine-Himalayan collision system, the Balkan belt to the north and the Dinarides-Hellenides belt to the South (e.g., Hsü et al. 1977). It has more recently been interpreted as an Alpine syn-metamorphic thrust complex based on new structural and geochronological studies (Burg et al. 1996; Ricou et al. 1998; Kilias and Mountrakis 1990; Ivanov et al. 2000; Mposkos and Krohe 2000; Krohe and Mposkos 2002; Liati 2005; Krenn et al. 2010). It occupies a central position in the Alpine belt, between the southwest-verging Hellenides and the north-verging Balkanides. The RD mostly consists of medium- to high-grade pre-Alpine and Alpine metamorphic rocks and granitoids and could represent the exhumed metamorphic core of the Alpine orogen of the Hellenides (Mposkos and Krohe 2000; Ivanov et al. 2000).The precise timing of the Alpine tectonometamorphic events remains poorly known for much of the RD; available geochronological data suggest a complex tectonometamorphic evolution spanning Jurassic to late Cenozoic times (e.g., Mposkos and Krohe 2000; Krohe and Mposkos 2002; Liati 2005; Cherneva and Georgieva 2005; Bonev et al. 2006; Bosse et al. 2009; Krenn et al. 2010). In the western RD (Pirin Mountains), probably Paleozoic kyanite eclogites occur in the Upper Allochthon (equivalent to Vertiskos complex of Mposkos and Krohe 2000) (Janak et al. 2011), which demonstrates the necessity of detailed age dating in this geodynamically complex region. Based on abrupt changes in metamorphic grade, Mposkos (1989) distinguished in the eastern Rhodope an upper tectonic unit of high-temperature eclogite-facies metamorphism (Kimi complex according to Mposkos and Krohe 2000) overprinted under upper amphibolite to granulite facies conditions, from a lower tectonic unit (Kechros complex according to Mposkos and Krohe 2000) of low-temperature eclogite-facies metamorphism overprinted under upper greenschist- to lower amphibolite-facies conditions.

In the Kimi Complex, eclogites have been described by Mposkos and Perdikatsis (1987), Liati and Mposkos (1990) and Bauer et al. (2007). In the Kechros Complex, detailed petrologic analysis of the various eclogitic rock types is limited (Mposkos and Perdikatsis 1987; Liati and Mposkos 1990).

The objective of this contribution is to establish a *P–T* path for the kyanite eclogite and common eclogites in the Kechros Complex of the eastern Rhodope. Segments of the path will be inferred from microtextures, mineral inclusions, mineral chemistry data and reaction histories present in these rocks. A basic understanding of the *P–T* history of the Kechros eclogites allows comparison with other known Alpine eclogites in the Rhodope Domain and the surrounding areas of the Aegean region and thus contributes to an understanding of the relative roles of these units during the Alpine orogeny, in particular, as more pertinent age data will become available in the future.

Geological setting

In the eastern Rhodope, a discrete tectonic contact separates the Kechros Complex from the overlying Kimi Complex (Fig. 1). The Kechros Complex consists of orthogneisses, reworked pre-Alpine migmatites (containing muscovite metapegmatite lenses), pelitic gneisses, high-alumina metapelites and very rare marbles. Large serpentinized peridotites are tectonically intercalated. These ultramafic bodies contain boudins of gabbroic pegmatites, diabase dykes, rodingitic gabbros and trondhjemites subsequently affected by HP metamorphism (Mposkos et al. 1997; Iliadis 2006). Within orthogneisses, serpentinites and between serpentinites and underlying metapelites boudins of eclogites, eclogite amphibolites and amphibolites occur.

HP metamorphism at *P–T* conditions of 1.4–1.5 GPa and 550–600°C was reported earlier from eclogites (Mposkos and Perdikatsis 1989; Liati and Mposkos 1990). In the orthogneisses and metapelites, the HP event is indicated by the presence of phengitic white K-mica reaching 3.50 and 3.43 Si atoms per formula unit (a.p.f.u.), respectively (Mposkos 1989). In metapelites, the formation of staurolite by the reactions $Cld + Ph \rightarrow St + Chl + Ms + Qz + H_2O$ and $Cld + Ms + Qz \rightarrow St + Bt + H_2O$ (abbreviations after Whitner and Evans 2010) suggests nearly isothermal decompression from maximum pressures of 1.4–0.4 GPa (Mposkos 1989; Mposkos and Liati 1993 in their Fig. 11), implying rapid uplift. At a later stage, at pressures below 0.3 GPa, andalusite is replacing chloritoid and green biotite is replacing garnet and muscovite. Orthogneisses and metapegmatites have Variscan protolith ages: In metapegmatites occurring in close association with a reworked migmatite, Rb–Sr dating of a large muscovite interpreted to be of magmatic origin yielded 334 Ma (Mposkos and Wawrzenitz 1995). U–Pb ages of magmatic zircons from orthogneisses range between 326 and 299 Ma (Peytcheva and von Quadt 1995; Liati 2005; Cornelius 2008). The precise timing of the HP tectonometamorphic event remains poorly known; 255-Ma U–Pb SHRIMP ages of magmatic zircons from the kyanite eclogite are interpreted as intrusion ages of the gabbroic protolith (Liati and Fanning 2005), indicating that the subsequent HP metamorphism is Alpine in age. Geochemical characteristics of this eclogite indicate a continental rifting environment for the gabbroic protolith (Liati and Fanning 2005; Baziotis and Mposkos 2010). A Rb–Sr age of large white K-mica (sieve fraction > 500 μm) from a mylonitic orthogneiss is 37 Ma (Wawrzenitz and Mposkos 1997). This is a minimum age of Alpine HP

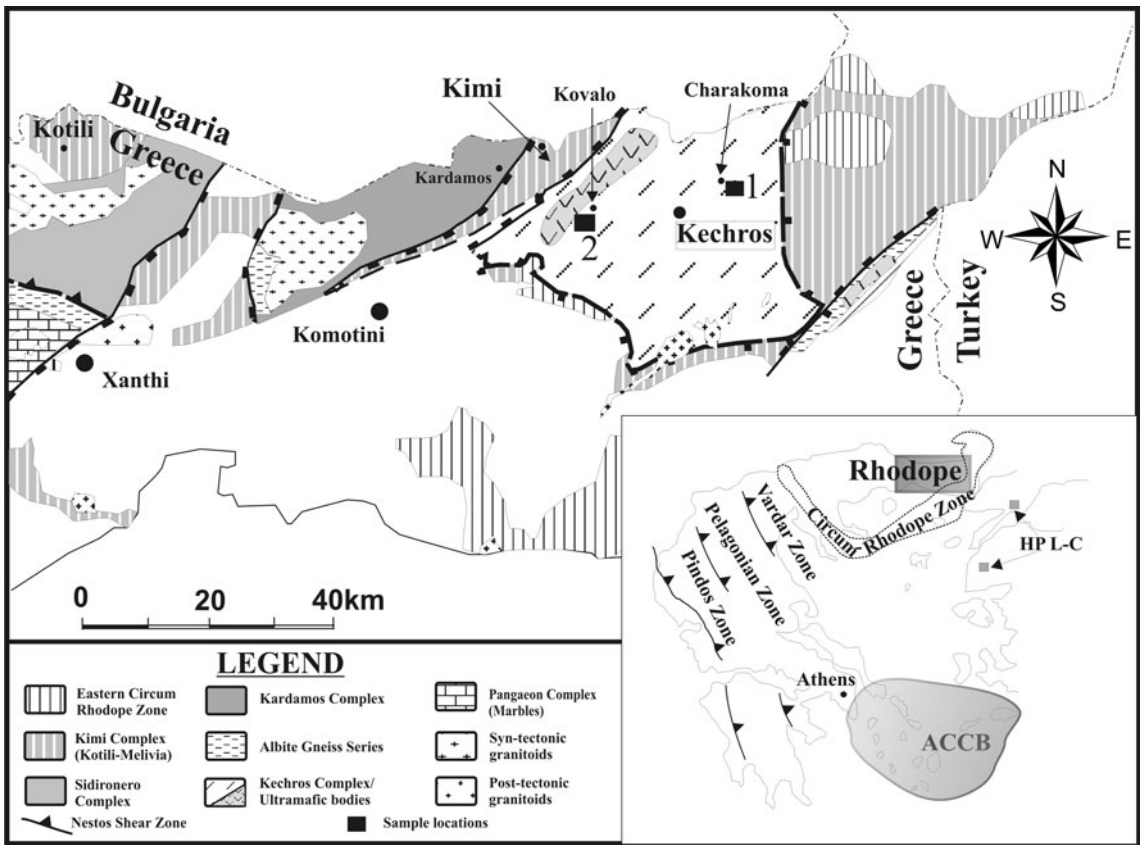

Fig. 1 Geological map of Central and East Rhodope in Greece (after Mposkos and Krohe 2000). *Numbers* indicate locations of the kyanite eclogite (*1*) and common eclogite (*2*) discussed in the present work. *Inset* Major tectonic zones in Greece. *ACCB* Attic-Cycladic Crystalline Belt. HP L-C: Late Cretaceous high-pressure rocks in East Thrace and Biga Peninsula of Turkey

metamorphism as in this sample such large white mica grains are essentially pre-mylonitic phengites crystallized during the HP metamorphism and deformed during the MP stage (Mposkos 1989; Wawrzenitz and Mposkos 1997). White micas from mylonitic orthogneisses yielded Ar/Ar ages of 36–42 Ma (Lips et al. 2000). Granodiorites and subvolcanic rocks that intruded the Kechros Complex, the overlying Kimi Complex and the Eocene basin sediments show Rb–Sr biotite ages between about 28 and 32 Ma (Del Moro et al. 1988), thus constraining the exhumation of the Kechros Complex to shallow crustal levels and extensional deformation between 36 and 32 Ma.

Field relations

The eclogites and retrogressed eclogites described in this paper are found in the Charakoma and Kovalo areas (Fig. 1). In the Charakoma area (coordinates 41°10′32N, 25°57′05.37″E), a kyanite eclogite body, lensoidal in shape (~200 m in length and ~40 m in thickness), is embedded in a garnet–phengite orthogneiss. On an outcrop scale, the main body of the eclogite is undeformed. However, discrete shear zones of post-eclogitic deformation, with garnet porphyroclasts in a fine-grained matrix consisting of hornblende, chlorite, epidote and biotite, are observed on a thin section scale under the petrographic microscope. At the margins, the eclogite is completely retrogressed into foliated and lineated amphibolite. The foliation of the surrounding phengite orthogneiss strikes NS and dips moderately toward the E. Foliation is defined by phengite and biotite flakes and stretching lineation by quartz ribbons.

In the Kovalo area (coordinates 41°12′40″N, 25°41′32″E), lenses of common eclogites 20–100 m in length occur within serpentinized peridotites and between foliated serpentinites and the underlying metapelites. Most of them are retrogressed to garnet amphibolites. Fresh eclogites occur only in the central parts of the lenses. No deformation textures can be observed in eclogites and their retrograde equivalents, suggesting that deformation during burial and exhumation to higher crustal levels was concentrated in the serpentinite and the surrounding metapelite. However, oriented rod-like titanite- and elongated amphibole grain inclusions in the garnets of some eclogite samples represent a pre-eclogitic stage of deformation.

Petrography and mineral chemistry

Two different high-pressure rock types are described herein: (1) kyanite eclogite (the eclogite of Charakoma area) and (2) common eclogite (the eclogites of Kovalo area; Fig. 1). The protolith of the kyanite eclogite was a low Fe–Ti gabbro, and those of the common eclogites were high Fe–Ti gabbros. Several whole-rock analyses were performed and published (Baziotis and Mposkos 2010). The range of values is given in Table 1, together with the specific analyses chosen for computing representative pseudosections for each rock type. Trace elements and REE patterns show a continental rifting environment for the protolith of the low Fe–Ti eclogite and an extensional oceanic environment for that of the high Fe–Ti eclogite (Baziotis and Mposkos 2010). The eclogites have experienced moderate to extensive retrogression after high-pressure metamorphism, with the typical increase in modal amount of amphibole, epidote/clinozoisite and plagioclase at the expense of pyroxene and garnet with increasing retrograde transformation, mainly toward the rims of lenses. Complete equilibration to amphibolite facies has led to entirely garnet-free assemblages at the outermost margins of eclogitic lenses. Estimated modal amounts of minerals in the studied eclogite and retrogressed eclogite samples are given in Table 2.

Analytical methods

Analyses were performed using a JEOL JSM G310 SEM equipped with a LINK ISIS energy-dispersive system and a MICROSPEC wave length dispersive system (for Na) at the Institute of Earth Sciences, University of Graz, and a JEOL 6380 LV SEM equipped with an energy-dispersive system (EDS) INCAx-Sight 7388 at the School of Mining and Metallurgical Engineering, National Technical University of Athens. Analytical conditions were 15-kV acceleration voltage and 5-nA probe current. Pyroxene nomenclature follows Morimoto (1988), while amphibole nomenclature is after Leake et al. (1997). Representative mineral analyses as well as compositions used for geothermobarometry are given in Tables 3, 4, 5 and 6.

Kyanite eclogite (samples EK-8, EK-9)

Based on thin section and SEM observations, the high-pressure assemblage in the kyanite eclogite is Grt + Omp + Na-Tr + Ky + Ph + Zo + Qz + Rt. Inclusions in garnet are abundant but unevenly distributed; most inclusions are omphacite, kyanite, quartz, amphibole, clinozoisite and rutile. Albite, phengite and paragonite inclusions are also present in the cores of the garnets, indicating that garnet started to grow before the *P–T* conditions reached the eclogite stage and continued to grow within the eclogite facies.

In Fig. 2a, the garnet contains inclusions of mainly quartz and amphiboles (Na-rich actinolite, winchite, barroisite, magnesiohornblende) and subordinate preiswerkite, staurolite and phengite. In Fig. 2b, the inclusions in garnet are quartz, omphacite and less clinozoisite and Al-rich tschermakite, and in Fig. 2c, they are predominantly kyanite, omphacite and quartz and only a few inclusions in the core of the garnet are albite and paragonite.

Garnet shows compositional growth zoning with increasing MgO and CaO and decreasing FeO and MnO from the core to the rim (see below Fig. 4a). The overall composition of garnet is in the range $Grs_{20–23}Prp_{18–30}Alm_{48–56}Sps_{0.8–2}$ (Table 3).

Matrix omphacite breaks down to symplectitic aggregates of hornblende + plagioclase (Fig. 2d). The composition of matrix clinopyroxene ranges from Jd_{24} to Jd_{54} (Table 4). Lower jadeite contents are found toward the

Table 1 Whole-rock compositions (wt%) of Kechros eclogites from East Rhodope

	Kyanite eclogite			Common eclogite		
	EK-9[+]	Average[a]	SD	93A-9[++]	Average[b]	SD
SiO_2	52.04	52.09	0.46	44.56	45.41	3.04
TiO_2	0.56	0.63	0.10	2.94	2.15	0.77
Al_2O_3	15.95	14.81	0.58	13.1	13.28	1.27
Fe_2O_3	8.18	8.58	0.64	18.7	15.60	3.34
MnO	0.14	0.14	0.04	0.27	0.23	0.04
MgO	8.96	8.99	1.65	6.76	8.37	0.93
CaO	9.03	9.24	0.61	10.87	11.67	1.46
Na_2O	1.80	2.17	0.46	2.53	1.92	0.97
K_2O	1.18	1.07	0.23	0.07	0.18	0.13
P_2O_5	0.13	0.14	0.04	0.17	0.16	0.06
LOI	0.95	1.57	0.47	0.1	0.58	0.48
Total	98.93	99.44	0.26	100.07	99.54	0.36

[+] Composition of kyanite eclogite used in pseudosection (Fig. 7a)

[++] Composition of common eclogite used in pseudosection (Fig. 7b)

[a] Average out of six analyses

[b] Average out of eight analyses

Table 2 Estimated modal mineral proportions (vol%) of the studied common, kyanite and retrograde eclogite samples from the Kechros complex

	Kyanite eclogite		Common eclogite		Retrograde eclogite	
	EK-8	EK-9	93A-8	93A-10	KO-6	93A-11
Grt	22	23	37	39	10	14
Omp	22	20	40	40	–	–
Di	–	–	–	–	3	4
Hbl	2	+	9	6	46	49
Tr/Act	30	34	3	4	11	4
Gln	–	–	1	1	+	+
Ky	2	3	–	–	–	–
Pl	7	4	3	4	20	23
Ep/Zo	2	3	3	2	5	5
Rt	+	+	2	2	2	1
Ilm	–	–	+	+	+	+
Ttn	–	–	1	1	1	+
Ph	6	7	–	–	2	+
Bt	2	2	–	–	+	+
Qz	4	3	+	+	+	+
Mrg	–	–	–	–	+	+
Prw	+	+	–	–	–	–
St	+	+	–	–	–	–
Pg	+	+	+	+	+	+

+ Traces (<1%)

rims of larger grains or in small grains associated with symplectitic hornblende + plagioclase aggregates, indicating a re-equilibration tendency to lower pressures during unloading. Armored inclusions of omphacite within garnet show the highest contents of Na_2O and Al_2O_3 (Table 4) and accordingly contain the highest jadeite content (up to 55 mol % Jd). Most analyses of omphacite inclusions are in the range Jd_{43}–Jd_{50}.

Kyanite inclusions in garnet are thin prisms up to 15 μm in longest diameter (Fig. 2c). Matrix kyanite (up to 100 μm long) is in textural equilibrium with matrix omphacite and phengite (Fig. 2d). It contains inclusions of garnet and omphacite.

Amphibole occurs in different textural and compositional variants. Amphibole inclusions in garnet are of two types: one is covering the composition range of Na-rich tremolite/actinolite, winchite, barroisite with Al_2O_3 content ranging from 3.93 to 7.74 wt% and Na_2O content from 1.56 to 3.60 wt% and the other one covers the range of Al-rich magnesiohornblende and tschermakite with Al_2O_3 content ranging from 14.5 to 17.4 wt% and Na_2O content from 2.0 to 3.24 wt%. The amphibole inclusions with high Al contents are observed in composite grain inclusions consisting of omphacite + high-Al amphibole + quartz or of low-Al and high-Al amphibole grains. They are interpreted as reaction products between Na-tremolite/omphacite inclusions and the garnet host formed during decompression.

The composition of matrix amphibole is widely variable (Table 5). Dominantly Na-rich tremolite/actinolite aggregates are pseudomorphically replacing primary (magmatic) pyroxene.

Figure 2e shows matrix amphibole with an actinolite core overgrown by Na-rich tremolite and then rimmed by omphacite + quartz, suggesting a prograde path with successive pressure increase.

Amphibole symplectitic with plagioclase replacing matrix omphacite is magnesiohornblende with Al_2O_3 content ranging from 7.22 to 10.83 wt%, and kelyphitic amphibole replacing garnet and omphacite is tschermakite with Al_2O_3 content ranging from 15.15 to 20.85 wt% (Fig. 2b). Tschermakite is also the matrix amphibole replacing Na-rich tremolite and garnet (Fig. 2a).

Phengite is a common phase with a flake size of 10–50 μm. At the rims, it is commonly replaced by biotite. Plagioclase + hornblende + biotite symplectites with relics of phengite indicate that phengite reacted with omphacite to form hornblende + plagioclase + biotite during decompression (Franz et al. 1986). The calculated Si content in phengites on the basis of 22 oxygen atoms, ($Fe^{+2} = Fe_{tot}$) varies between 6.64 and 6.80. Compositions of phengite and biotite are given in Table 6.

Plagioclase inclusions in garnet are pure albite. Matrix plagioclase is oligoclase/andesine with An content ranging from 26 to 36%. Clinozoisite inclusions in garnet and matrix clinozoisite show similar Fe_2O_3 contents ranging from 2.6 to 6.7 wt% (Table 6).

Paragonite is found only as inclusions in the cores of garnets (Fig. 2c). Preiswerkite, staurolite and phengite were

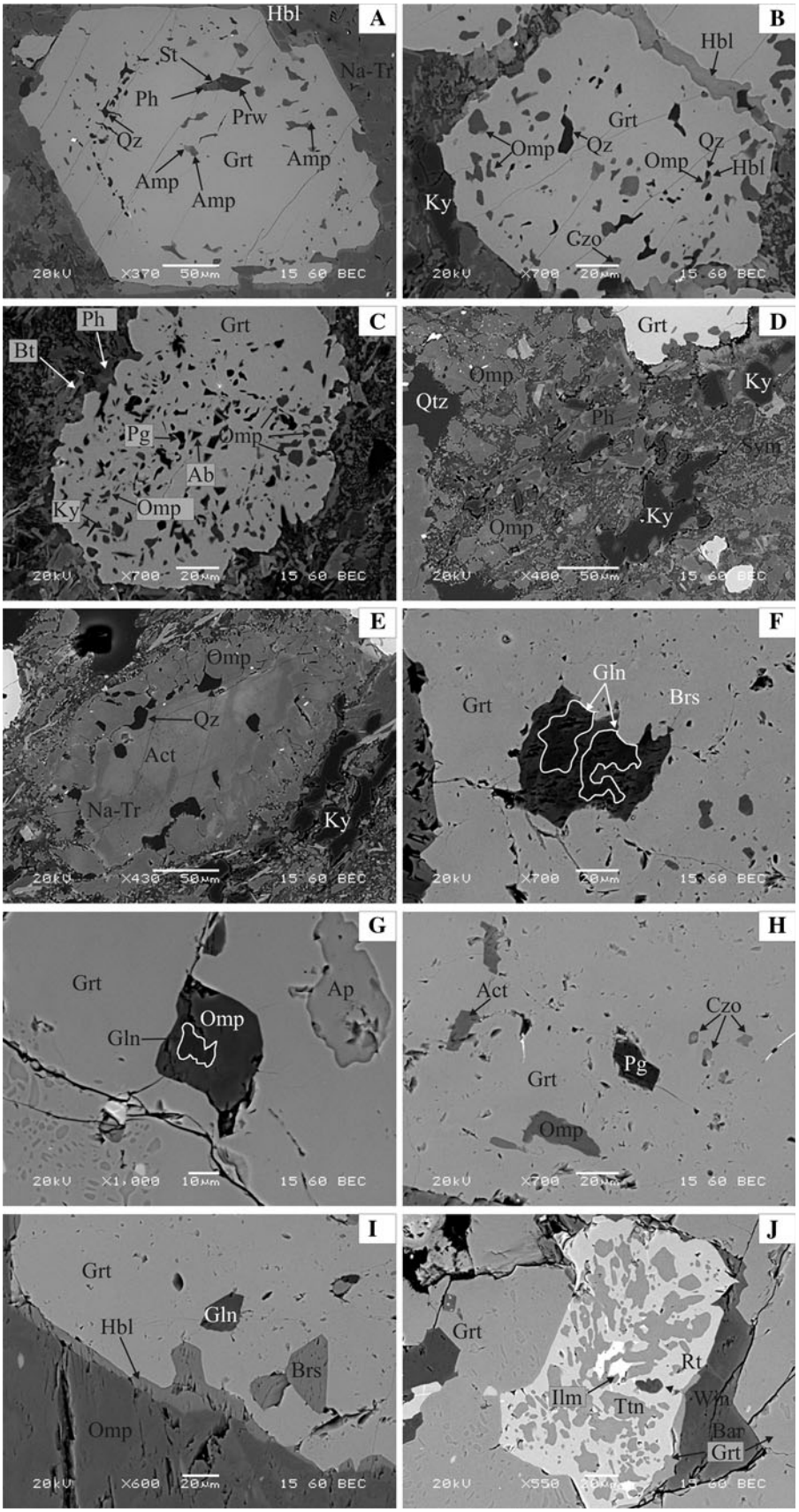
A
Hbl
St
Na-Tr
Ph
Prw
Qz
Grt
Amp
Amp
Amp
B
Hbl
Grt
Omp
Qz
Qz
Omp
Hbl
Ky
Czo
C
Ph
Grt
Bt
Pg
Omp
Ab
Ky
Omp
D
Grt
Omp
Ky
Qtz
Ph
Sym
Omp
Ky
E
Omp
Qz
Act
Na-Tr
Ky
F
Gln
Grt
Brs
G
Grt
Ap
Omp
Gln
H
Act
Czo
Pg
Grt
Omp
I
Grt
Gln
Hbl
Brs
Omp
J
Grt
Rt
Ilm
Ttn
Wm
Bar
Grt

◀ **Fig. 2** BSE images of kyanite eclogite (**a**–**e**) and common eclogite (**f**–**j**): **a** Garnet (*Grt*) with inclusions of sodic actinolite, winchite, barroisite (*Amp*), phengite (*Ph*), preiswerkite (*Prw*), staurolite (*St*) and quartz (*Qz*). The matrix consists of Na-rich tremolite grains (Na-Tr) rimmed by tschermakite (Hbl). **b** Garnet with inclusions of Ca-amphibole (*Hbl*), quartz, omphacite (*Omp*) and clinozoisite (*Czo*). Garnet shows corroded edges and is replaced by tschermakitic hornblende. Matrix omphacite is associated with kyanite (*Ky*). Matrix omphacite is decomposed to hornblende + plagioclase symplectites. **c** Garnet rich in inclusions of omphacite, kyanite and quartz. Albite (Ab) and paragonite (Pg) inclusions are present in the core of the garnet. Matrix phengite is rimmed by biotite, and matrix omphacite is replaced by hornblende + plagioclase symplectites. **d** Peak pressure assemblage consisting of omphacite + phengite + kyanite + garnet + quartz together with retrograde hornblende + plagioclase + biotite symplectites (*Sym*) replacing omphacite and phengite. **e** Actinolite (*Act*) is replaced patchily and at the rims by Na-rich tremolite (Na-Tr) and is mantled by omphacite + quartz aggregates. **f** Composite grain inclusion in garnet consisting of glaucophane (*Gln*) and barroisite (*Brs*). Barroisite seems to replace the glaucophane. **g** Inclusion of omphacite in garnet. The omphacite inclusion contains an inclusion of glaucophane. *Ap* apatite inclusion. **h** Inclusions of paragonite, sodic actinolite, omphacite and clinozoisite (*Czo*) in garnet. **i** Garnet + matrix omphacite assemblage. Between garnet and omphacite, kelyphitic Al-rich ferro-barroisite (*Hbl*) is formed. Garnet contains inclusions of glaucophane and (retrograde) Al-rich ferro-barroisite (*Brs*). **j** Rutile (*Rt*) with inclusions of ilmenite (*Ilm*), titanite (*Ttn*) and winchite (*Wnc*) is associated with garnet. Garnet contains numerous inclusions of titanite

found as a composite grain inclusion only in one garnet (Fig. 2a). They probably are the decomposition products of a former K-bearing paragonite + chloritoid composite inclusion that reacted during decompression. The composition of the sodic trioctahedral mica represents solid solution with 10% paragonite and 90% preiswerkite component (Table 6). The Fe/(Fe + Mg) ratio in staurolite is 0.73.

Common eclogite (samples 93A8–93A10)

Based on thin section and SEM observations, the high-pressure assemblage in the common eclogite is Grt + Omp + (?Gln) + Rt. Garnet (major constituent up to 40 vol%) forms aggregates of subhedral grains of 0.05–0.8 mm in diameter. Garnet contains inclusions of omphacite, amphiboles, clinozoisite, titanite and rutile and most rarely of paragonite, albite and apatite. Single-grain amphibole inclusions in garnet are glaucophane, Na-rich actinolite, magnesiohornblende, winchite and barroisite. Some glaucophane inclusions in garnet are transformed into barroisite or rimmed by omphacite (Fig. 2f, g).

Garnet shows compositional zoning with core composition $Alm_{57–61}Prp_{2–3}Grs_{32–33}$ $Sps_{.4–.7}$ and rim composition $Alm_{61–63}Prp_{8–11}Grs_{26–27}Sps_{0.6–0.7}$. Omphacite (major constituent 30 to 40 vol%) forms prismatic crystals up to 1.2 mm long and contains rare single-grain inclusions of Ca-amphibole, glaucophane, garnet and rutile or aggregates of rutile and titanite. Large omphacite grains show, in BSE image, darker and brighter patches that differ in their chemical composition. The darker patches show higher jadeite component ($Jd_{38–40}$) than the brighter ones ($Jd_{28–31}$). Omphacite occurs also as inclusions in garnet (Fig. 2g, h) with jadeite components ranging from Jd_{26} to Jd_{38}.

Diopside occurs in symplectitic intergrowth with albite ($An_{0–2}$) replacing omphacite. The jadeite component in diopside ranges from Jd_6 to Jd_{14} (Table 4).

Glaucophane occurs only as inclusions, commonly in garnet and most rarely in omphacite. It is also found as inclusion in matrix Ca-amphibole of retrogressed eclogite, suggesting that glaucophane was present as a matrix phase in the eclogite stage, even though its presence at peak conditions remains uncertain from textural evidence. Representative analyses are shown in Table 5. Calcic and sodic-calcic amphiboles occur in different textural and compositional variations. Amphibole inclusions in garnet are of two types: type 1 includes single grains of glaucophane and Na-actinolite/winchite with Al_2O_3 content up to 7.43 wt% and type 2 includes Ca- and Na–Ca-amphiboles with Al_2O_3 content ranging from 12 to 19 wt% (Table 5; Fig. 6). Al-rich Ca- and Na–Ca-amphiboles occur in composite grain inclusions in garnet replacing inclusions of glaucophane (Fig. 2f), Na-rich actinolite or omphacite. Commonly fractures in the garnet host lead to the inclusions suggesting that fluid intrusion triggered the reaction between glaucophane, Na-rich actinolite or omphacite inclusion and garnet host to form the Al-rich Ca- and Na–Ca-amphiboles during decompression.

Plagioclase inclusions in garnet are pure albite. Paragonite is also found only as inclusion in garnet (Fig. 2h). The Fe_2O_3 content in epidote/clinozoisite inclusions in garnet ranges from 8.44 to 10.46 wt% (Table 6).

Rutile up to 0.2 mm in size contains inclusions of ilmenite (Ilm-1), titanite (Ttn-1), commonly with corroded edges, and rarely barroisite (Al_2O_3 = 6.95 wt%) and is in textural equilibrium with garnet (Fig. 2j). The associated garnet contains numerous small inclusions of titanite and epidote. We interpret this texture as pseudomorphs of former (magmatic) ilmenite that is replaced by titanite at the first stage of the prograde path of metamorphism, and at a second stage, at higher pressures, titanite and epidote reacted to form garnet and rutile. Rutile also occurs as inclusions in garnet and omphacite.

Retrogressed common eclogite (samples KO-6, 93A-11)

Textures and mineral compositions in intensely retrogressed eclogites from the Kovalo area give additional information about the decompression *P*–*T* path. We include, in the present, work samples KO-6 and 93A-11 with the mineral assemblage: Grt + Ca-Amp + Gln + Zo/Czo + Ph +Pg + Mrg + Pl + Bt + Ilm + Ttn. Glaucophane (Table 5) is

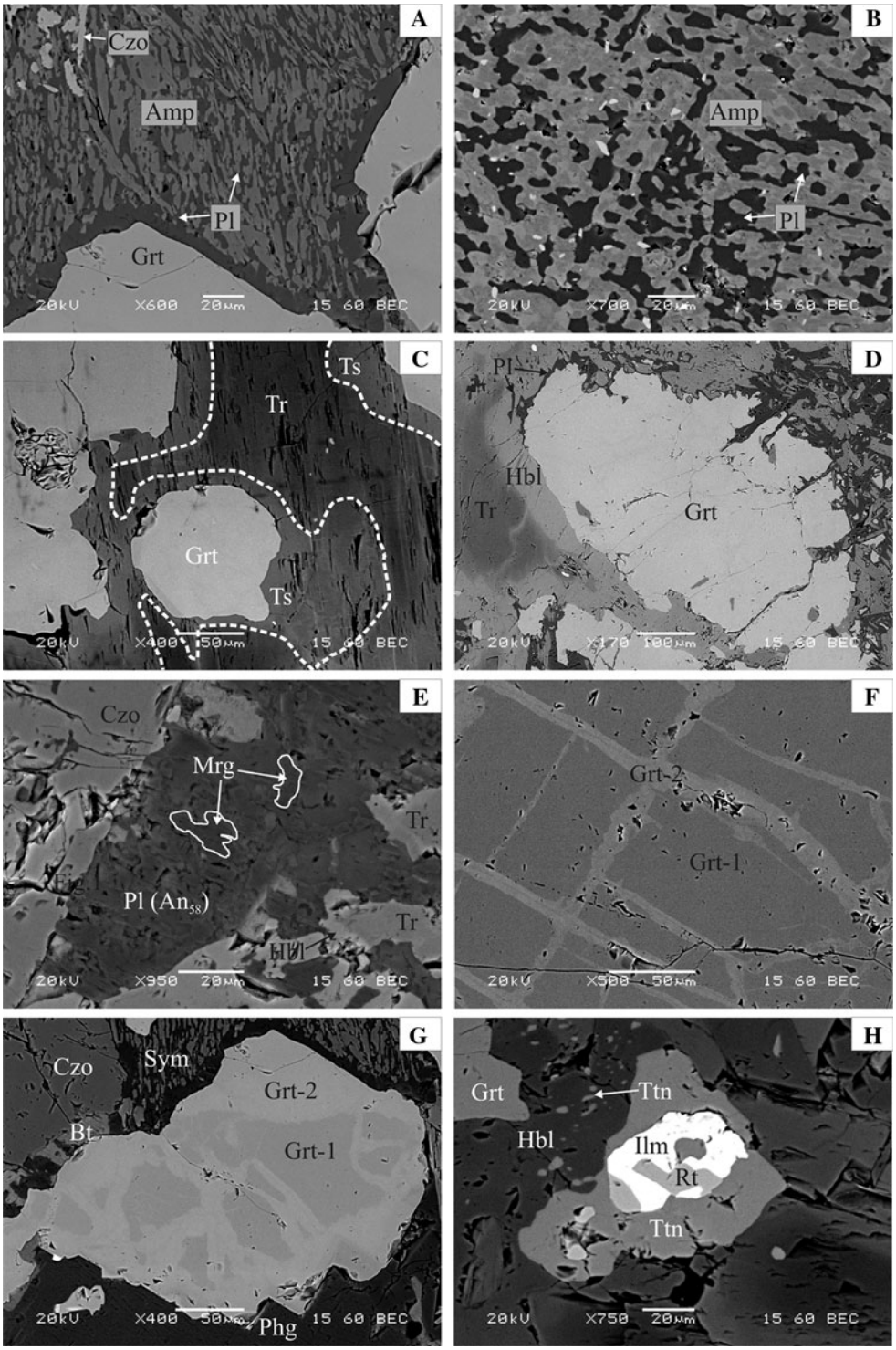

Fig. 3 Retrogressed eclogite (Sample KO-6). **a** Hornblende-plagioclase symplectites replacing former omphacite. **b** Close-up of symplectite showing that low-Al amphibole (*gray*) is overgrown by high-Al amphibole (*light gray*). **c** Zoned matrix Ca-amphibole. The tremolite core is replaced by tschermakite (Al_2O_3 = 2.33 and 19.48 wt%, respectively, Table 5 analyses 53 and 54). **d** Kelyphitic Al-rich tschermakite replaces sodic tremolite and garnet. **e** Margarite inclusions in plagioclase. **f**, **g** Two generations of garnet. The first generation of the eclogite stage (Grt-1) is replaced by Grt-2 along grain boundaries, cracks and veins. **h** Matrix rutile is replaced by ilmenite (*Ilm*) and both phases by titanite (*Ttn*)

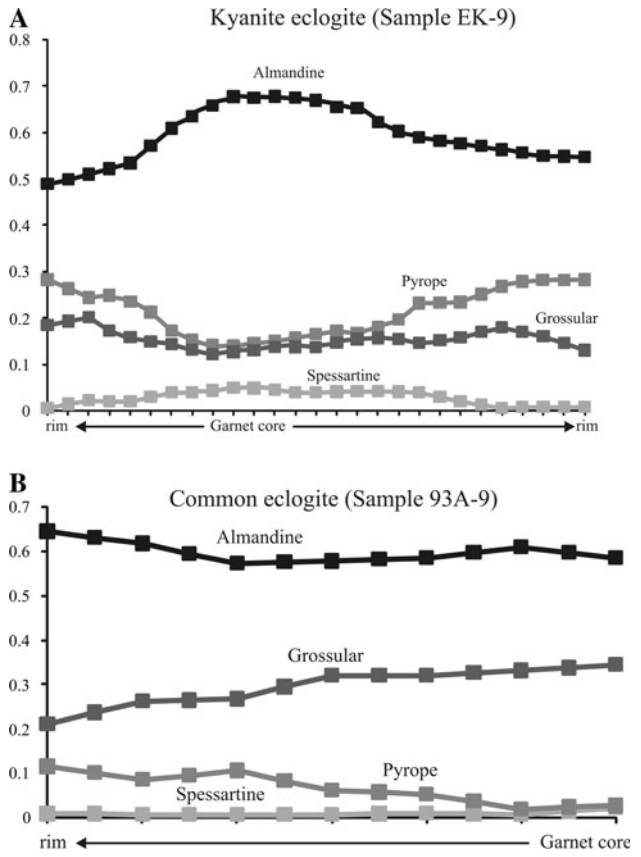

Fig. 4 Chemical zoning pattern of garnet crystals from **a** kyanite eclogite (rim–rim) and **b** common eclogite (core–rim)

a relic of the prograde or peak metamorphic stage and observed as armored inclusions in retrograde matrix tremolite. Paragonite is also observed only as inclusions in matrix magnesiohornblende. Omphacite is completely transformed into symplectites of Ca-amphibole + plagioclase ($An_{13–26}$) during decompression (Fig. 3a, b). This amphibole is actinolite to magnesiohornblende with Al_2O_3 content ranging from 3 to 11 wt%. Symplectitic plagioclase with the lower An component ($An_{13–17}$) coexists with actinolite with Al_2O_3 content ranging from 3 to 5 wt%, while symplectitic plagioclase with higher An content ($An_{22–26}$) coexists with hornblende showing higher Al_2O_3 (8–11 wt%). Matrix amphiboles show compositional zoning with Na-tremolite/actinolite core composition (Al_2O_3 ranging from 2.33 to 5.43 wt%) and magnesio-hornblende, Al-rich ferro-barroisite to magnesiohastingsite rim composition (Al_2O_3 ranging from 11.76 to 19.48 wt%) (Table 5). The highest Al_2O_3 contents are found in kelyphitic and diablastic amphiboles replacing garnet and Na-tremolite/actinolite or omphacite during decompression (Table 5; Figs. 2i, 3c, d). Kelyphitic amphibole replacing garnet and tremolite (Fig. 3d) near the garnet rim has the composition of Al-rich tschermakite (Al_2O_3 up to 21 wt%).

Margarite is observed as inclusion in clinozoisite and as armored relics in An-rich plagioclase of the matrix (Fig. 3e). Representative compositions are given in Table 6. Margarite is Na rich with up to 37% paragonite and 5% muscovite component. Matrix margarite is decomposed to plagioclase ($An_{50–58}$) (Fig. 3e), and phengite (Si = 6.79–6.95 a.p.f.u.) is replaced by biotite + plagioclase ($An_{36–44}$) symplectites after reaction with omphacite.

Eclogitic garnet (Grt-1) is replaced by a new garnet (Grt-2; Fig. 3f, g) that differs strongly in chemical composition from the eclogitic garnet (Table 3). The composition of Grt-1 is $Grs_{32}Prp_8Alm_{59}Sps_1$ in the core and $Grs_{29}Prp_{15}Alm_{55}Sps_1$ at the rim, and that of Grt-2 is $Grs_{38}Prp_{0.0}Alm_{42}Sps_{20}$ in the core and $Grs_{38}Prp_4Alm_{49}Sps_9$ at the rim. Inclusions of biotite, plagioclase (An_{36}), epidote and Al-rich tschermakitic hornblende (Al_2O_3 18.06 wt%), similar in composition to the matrix kelyphitic hornblende, in Grt-2 indicate that it was formed during decompression. The prograde growth zoning of Grt-2, the compositional zoning of the matrix amphiboles with increasing Al_2O_3 content from the core to the rim (Table 5) and the association of matrix albite with oligoclase/andesine in the retrogressed eclogite samples could be interpreted to record the transition from the albite–epidote–amphibolite facies to amphibolite facies accompanied by a temperature increase at this stage of decompression. But as these compositional differences occur on a thin section scale and particularly Al-rich and Al-poor assemblages are bound to domains that are defined by the decomposition of Al-rich and Al-poor eclogite facies minerals, a more likely interpretation is that equilibrium has not been attained on a millimeter scale and that the observed growth zoning reflects growing volumes of equilibration rather than changes in *P–T* conditions.

Petrological interpretation and *P–T* evolution

Mineral zoning and mineral composition related to prograde growth

Garnet zoning

The zoning characteristics of the eclogitic garnets from the kyanite eclogite and the common eclogite from the Kechros Complex are shown in Fig. 4a and b, respectively. The increase in pyrope and the decrease in grossular and spessartine component from the core to the rim of the garnet from the common eclogite (Fig. 4b) implies prograde growth zoning. The garnet profile from the kyanite eclogite shows more complex zoning (Fig. 4a). From core to rim, the pyrope component increases while the almandine and spessartine components decrease and the grossular component shows first an increase and then a decrease. The

Table 3 Representative microprobe analyses of garnet from Kechros eclogites

Rock type	Kyanite eclogite					Common eclogite			
#Analysis	89-core	84-rim	57-rim	127[a]	130[a]	66-core	45-rim	71[a]	74[a]
SiO_2	37.60	38.90	38.70	38.40	38.45	37.52	37.58	37.69	37.5
TiO_2	–	–	–	–	–	–	–	–	–
Al_2O_3	21.10	21.19	21.25	21.67	21.62	20.28	20.47	20.23	20.77
FeOt	31.76	23.12	25.02	24.53	25.81	27.86	31.18	25.16	26.30
MnO	1.69	0.30	0.31	0.81	1.02	–	–	3.84	2.91
MgO	3.34	7.39	7.33	5.60	5.53	1.01	3.17	1.79	0.91
CaO	4.47	8.02	7.06	8.36	7.43	13.01	7.17	10.94	11.4
Total	99.96	98.92	99.67	99.37	99.86	99.68	99.57	99.65	99.79
Oxygens	12								
Si	3.001	3.000	2.993	2.999	2.998	2.997	3.000	3.009	3.000
Ti	–	–	–	–	–	–	–	–	–
Al	1.985	1.926	1.938	1.995	1.987	1.909	1.927	1.903	1.958
Fe^{+2}	2.119	1.533	1.610	1.602	1.683	1.850	2.074	1.680	1.759
Mn	0.114	0.020	0.020	0.054	0.067	–	–	0.260	0.197
Mg	0.397	0.860	0.845	0.652	0.643	0.121	0.377	0.213	0.109
Ca	0.382	0.663	0.585	0.700	0.621	1.113	0.613	0.936	0.977
Rock type	Retrogressed common eclogite								
#Analysis	101-1c	102-1r	37-1c	38-1r	22-2c	23-2r	11n-2c	12n-2r	2
SiO_2	37.87	38.03	38.19	38.14	37.55	37.66	37.59	37.73	37.65
TiO_2	–	–	–	–	–	–	–	–	–
Al_2O_3	20.09	21.48	20.39	21.3	20.52	20.62	21.13	20.73	20.42
FeOt	26.57	25.80	22.77	22.83	19.73	21.43	20.00	21.24	20.58
MnO	0.5	0.3	1.09	1.62	7.76	5.58	7.23	5.73	7.27
MgO	2.16	3.72	3.65	3.04	0.91	1.1	0.32	1.26	0.62
CaO	12.45	10.35	13.33	12.83	13.09	13.34	13.98	12.88	13.23
Total	99.64	99.68	99.42	99.76	99.56	99.73	100.25	99.57	99.77
Oxygens	12								
Si	3.007	2.988	2.998	2.992	2.998	2.997	2.983	3.004	3.006
Ti	–	–	–	–	–	–	–	–	–
Al	1.880	1.989	1.887	1.969	1.931	1.934	1.977	1.946	1.922
Fe^{+2}	1.764	1.695	1.495	1.498	1.318	1.426	1.327	1.415	1.374
Mn	0.034	0.020	0.072	0.108	0.525	0.376	0.486	0.386	0.492
Mg	0.256	0.436	0.427	0.355	0.108	0.130	0.038	0.150	0.074
Ca	1.059	0.871	1.121	1.078	1.120	1.137	1.189	1.099	1.132

[a] In contact with omphacite inclusion

higher almandine and the lower pyrope component in the garnet of the common eclogite, compared to that of the kyanite eclogite, may probably be attributed to the bulk rock chemical compositions of the protoliths and less to *P–T* conditions (see chapter on *P–T* conditions below).

Pyroxene composition

There are no significant compositional differences between the clinopyroxene inclusions in garnet and matrix clinopyroxenes. In the kyanite eclogite, the jadeite component in clinopyroxene inclusions in the garnet ranges from Jd_{43} to Jd_{55} and in the matrix clinopyroxenes from Jd_{24} to Jd_{54}. In the common eclogite, the jadeite component in clinopyroxene inclusions in garnet is Jd_{26} to Jd_{38} and in the matrix clinopyroxene from Jd_{24} to Jd_{40}. The acmite component in clinopyroxene of the high Fe–Ti common eclogite is higher than that in clinopyroxene of the low Fe–Ti kyanite eclogite (Fig. 5).

The higher jadeite content in clinopyroxene from the kyanite eclogite compared to that of the common eclogite could indicate clinopyroxene formation at higher pressures

Table 4 Representative microprobe analyses of clinopyroxene from Kechros eclogites

Rock type	Kyanite eclogite					Common eclogite				
#Analysis	10/M	51/i	55/i	126/i	129/i	35/i	15	70/i	80	76
SiO_2	56.59	54.69	55.02	55.89	56.16	54.73	54.89	55.18	55.38	53.68
TiO_2	–	–	–	–	–	–	–	–	–	–
Al_2O_3	12.46	11.6	12.8	11.69	12.50	7.84	9.29	9.02	9.58	1.40
FeO_T	3.33	6.22	6.17	5.26	4.93	9.24	6.79	8.89	5.54	
MnO	–	–	–	–	–	–	–	–	–	–
MgO	8.29	6.21	6.83	6.49	6.94	7.51	7.47	7.32	7.76	13.41
CaO	12.16	14.28	11.74	12.5	11.55	12.57	14.67	12.47	13.91	21.77
Na_2O	7.42	7.02	6.99	7.33	8.1	6.78	5.93	6.69	6.72	1.47
Total	100.25	100.02	99.55	99.16	100.18	98.67	99.04	99.57	98.89	98.96
Oxygens	6									
Si	1.999	1.958	1.972	2.008	1.980	1.999	1.999	1.998	2.000	1.998
Ti	–	–	–	–	–	–	–	–	–	–
Al	0.497	0.489	0.541	0.495	0.520	0.338	0.399	0.385	0.408	0.061
Fe^{3+}	0.013	0.000	0.000	0.016	0.034	0.143	0.019	0.085	0.059	0.045
Fe^{2+}	0.085	0.186	0.185	0.142	0.111	0.140	0.188	0.184	0.108	0.180
Mn	–	–	–	–	–	–	–	–	–	–
Mg	0.436	0.331	0.365	0.348	0.365	0.409	0.405	0.395	0.418	0.744
Ca	0.460	0.548	0.451	0.481	0.436	0.492	0.572	0.484	0.538	0.868
Na	0.508	0.487	0.486	0.511	0.554	0.480	0419	0.470	0470	0.106

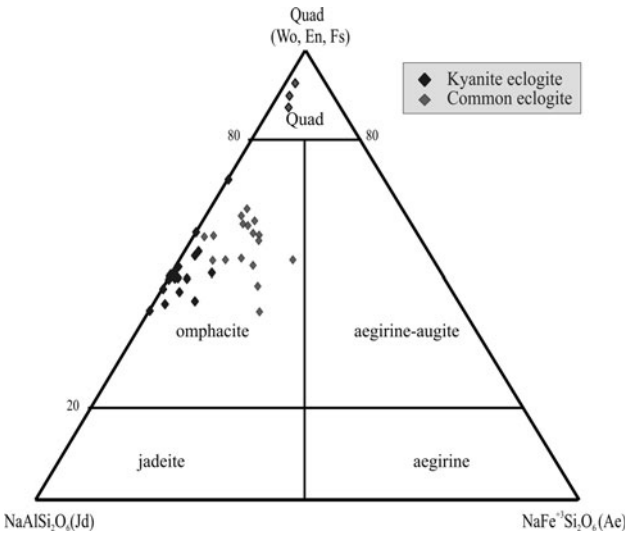

Fig. 5 Compositional variation in sodic pyroxene from eclogites of the Kechros complex plotted in Quad-Jd-Ae ternary diagram. End-member components are calculated according to Morimoto (1988)

(Fig. 5). The presence of paragonite inclusions in the garnets of both eclogite types and the absence of kyanite in the common eclogite may support this assumption. However, both observations could also be attributed to differences in the bulk rock composition—a question we have tried to answer by the analysis of isochemical phase diagram sections (pseudosections) below.

Amphibole composition

In kyanite eclogite, the amphibole inclusions in garnet and the matrix amphiboles which occur in textural equilibrium with omphacite are Na-rich tremolite to winchite or barroisite with Si 7.5–6.5 a.p.f.u. and Na_B 0.35–0.8 a.p.f.u. (Fig. 6a).

In the common eclogite, the amphibole inclusions in garnet are glaucophane with Si 7.8–7.9 a.p.f.u. and Na_B 1.6–1.9 a.p.f.u., Ca-poor magnesiohornblende, winchite and barroisite with Si 7.2–7.7 a.p.f.u. and Na_B 0.25–0.7 a.p.f.u. (Fig. 6a). The compositions of prograde Ca- and Na–Ca-amphiboles (single-grain inclusions in garnet in both the kyanite eclogite and common eclogite and the matrix Na-rich tremolite in the kyanite eclogite) plot within the compositional range indicated by Laird and Albee (1981) for high-pressure metabasites. The amphibole compositions from composite grain inclusions plot outside from the high-pressure field (Fig. 6b, c), most of them within the compositional range of the medium pressure. They are probably reaction products between Na-tremolite or omphacite inclusions and the garnet host formed during decompression.

Mineral inclusions

Solid inclusions are abundant in the garnet of the kyanite and common eclogite and provide valuable information on

Table 5 Representative microprobe analyses of amphiboles from Kechros eclogites

Rock type	Kyanite eclogite						Common eclogite			
#Analysis	55/M	58/Kel	59/M	64/Sym	66i	109i	24/i	65/i	44/i	52/i
SiO_2	56.82	41.49	56.09	53.43	56.26	53.50	39.37	50.25	52.76	57.50
TiO_2	–	–	–	–	–	–	–	–	–	–
Al_2O_3	4.62	20.77	4.40	7.22	7.74	7.15	19.08	10.55	6.73	9.69
FeO	4.96	13.17	5.85	5.66	6.35	8.20	20.31	14.79	11.01	10.77
MnO	–	–	–	–	–	–	–	–	–	–
MgO	19.01	8.44	18.80	17.87	16.14	15.95	4.67	10.07	15.21	10.86
CaO	10.22	9.60	10.24	11.01	7.43	10.23	9.67	8.93	8.54	1.37
Na_2O	1.88	3.88	1.89	1.96	3.60	2.58	3.26	3.20	2.62	6.73
K_2O	–	–	–	–	–	–	–	–	–	–
Total	97.51	97.35	97.27	97.15	97.52	97.61	96.36	97.79	96.87	96.92
Oxygens	23									
Si	7.796	6.022	7.741	7.444	7.719	7.514	5.965	7.253	7.409	7.942
Ti	–	–	–	–	–	–	–	–	–	–
Al^{IV}	0.204	1.978	0.259	0.556	0.281	0.486	2.035	0.747	0.591	0.058
Al^{VI}	0.543	1.575	0.457	0.629	0.970	0.697	1.372	1.048	0.523	1.520
Fe^{+3}	0.156	0.322	0.267	0.111	0.168	0.008	0.559	0.041	0.771	0.328
Fe^{+2}	0.412	1.276	0.408	0.548	0.560	0.955	2.014	1.744	0.521	0.916
Mn	–	–	–	–	–	–	–	–	–	–
Mg	3.888	1.826	3.868	3.711	3.301	3.340	1.055	2.167	3.184	2.236
Ca	1.502	1.493	1.514	1.643	1.092	1.539	1.570	1.381	1.285	0.203
Na^B	0.498	0.507	0.486	0.357	0.908	0.461	0.430	0.619	0.713	1.797
Na^A	0.002	0.585	0.020	0.173	0.050	0.242	0.527	0.276	–	0.005
K	–	–	–	–	–	–	–	–	–	–

Rock type	Common eclogite	Retrogressed common eclogite								
#Analysis	27/Kel	1/M-core	2/M-rim	47/M-core	46/Kel-rim	53/core	54/rim	61/i[a]	23/Sym	35
SiO_2	43.93	51.96	40.09	54.53	40.43	55.41	40.65	58.09	51.57	54.51
TiO_2	–	–	–	–	–	–	–	–	–	–
Al_2O_3	15.28	4.36	19.56	7.00	20.21	2.33	19.48	11.30	7.86	5.85
FeO	17.78	12.70	17.24	8.19	16.59	6.42	16.77	6.60	10.10	7.57
MnO	–	–	–	–	–	–	–	–	–	–
MgO	7.51	14.88	6.40	15.89	6.95	19.89	7.15	12.92	14.96	17.07
CaO	8.54	12.36	11.16	10.15	11.18	12.47	11.92	1.88	11.69	10.23
Na_2O	3.63	0.30	2.65	1.96	1.94	0.50	1.39	6.60	0.97	1.75
K_2O	–	–	–	–	–	–	–	–	–	–
Total	96.67	96.56	97.10	97.72	97.30	97.02	97.36	97.39	97.15	96.98
Oxygens	23									
Si	6.490	7.514	5.984	7.596	5.940	7.731	5.985	7.851	7.320	7.605
Ti	–	–	–	–	–	–	–	–	–	–
Al^{IV}	1.510	0.486	2.016	0.404	2.060	0.269	2.015	0.149	0.680	0.395
Al^{VI}	1.150	0.257	1.424	0.746	1.440	0.114	1.365	1.651	0.635	0.566
Fe^{+3}	0.609	0.314	0.255	0.099	0.542	0.291	0.487	0.223	0.221	0.296
Fe^{+2}	1.587	1.222	1.897	0.855	1.497	0.458	1.578	0.523	0.978	0.588
Mn	–	–	–	–	–		–	–	–	–
Mg	1.654	3.208	1.424	3.300	1.522	4.137	1.569	2.603	3.166	3.550
Ca	1.352	1.915	1.784	1.515	1.760	1.864	1.880	0.272	1.778	1.529
Na^B	0.648	0.084	0.216	0.485	0.240	0.135	0.120	1.728	0.222	0.471
Na^A	0.391	–	0.551	0.044	0.312	0.000	0.277	0.002	0.045	0.002
K	–	–	–	–	–	–	–	–	–	–

[a] Inclusion in matrix amphibole

Table 6 Representative microprobe analyses of phengite, biotite, preiswerkite, staurolite, plagioclase, epidote, margarite ilmenite and titanite from Kechros eclogites

Rock type	Kyanite eclogite							Common eclogite		
#Analysis	Ph-13	Bt-14	Prw	St-64/i	Pl-15 M	Pl-32sym	Ep-9 M	Ep-32i	Ep-16i	Ab-10sym
SiO_2	49.32	37.99	30.11	27.61	58.92	63.14	39.50	38.98	58.78	68.65
TiO_2	0.19	0.32	–	–	–	–	–	–	–	–
Al_2O_3	29.03	21.69	36.66	56.27	26.49	23.38	31.76	28.70	27.51	19.33
FeO	2.20	8.97	6.15	12.63	–	–	2.67*	6.66*	8.44*	–
MnO	–	–	–	–	–	–	–	–	–	–
MgO	3.08	15.79	14.47	2.18	–	–	–	–	–	–
CaO	–	–	–	–	6.87	4.51	24.57	24.16	24.06	–
Na_2O	–	–	7.16	–	7.74	8.76	–	–	–	11.77
K_2O	11.07	10.13	–	–	–	–	–	–	–	–
Total	94.90	94.90	94.56	98.70	100.02	99.80	98.50	98.50	98.80	99.75
Oxygens	22	22	22	47	8	8	12.5	12.5	12.5	8
Si	6.626	5.489	4.174	7.700	2.625	2.791	3.002	3.006	3.001	3.003
Ti	0.019	0.035	–	–	–	–	–	–	–	–
Al^{IV}	1.374	–	3.826	0.300	1.391	1.218			–	0.996
Al^{VI}	3.223	3.693	2.164	18.198	–	–	2.844	2.608	2.509	–
Fe^{+3}	–	–	–	–	–	–	0.153	0.386	0.492	–
Fe^{+2}	0.248	1.083	0.714	2.947	–	–	–	–	–	–
Mn	–	–	–	–	–	–	–	–	–	–
Mg	0.618	3.399	2.990	0.906	–	–	–	–	–	–
Ca	–	–	–	–	0.328	0.213	2.000	1.996	1.996	–
Na	–	–	1.927	–	0.669	0.751	–	–	–	0.999
K	1.897	1.867	–	–	–	–	–	–	–	–

Rock type	Common eclogite			Retrogressed common eclogite						
#Analysis	Pl-75sym	Ilm-26	Ttn-27	Ep-31	Ep-86	Mrg-81	Pl-82	Pl-18 Symp	Pl-38	Pl-67
SiO_2	66.16	–	36.60	39.51	39.30	36.24	54.03	63.00	60.13	65.91
TiO_2	–	52.83	40.01	–	–	–	–	–	–	–
Al_2O_3	20.85	–	0.35	32.99	32.37	46.17	29.04	22.78	25.08	21.10
FeO	–	46.46	–	0.96*	1.63*	0.96	–	–	–	–
MnO	–	–	–	–	–	–	–	–	–	–
MgO	–	0.50	–	–	–	–	–	–	–	–
CaO	2.66	–	28.62	24.74	24.30	8.13	11.93	5.49	6.88	3.61
Na_2O	10.20	–	–	–	–	2.91	4.80	8.50	7.87	9.58
K_2O	–	–	–	–	–	0.62	–	–	–	–
Total	99.87	99.80	99.60	98.20	97.60	95.02	99.80	99.77	99.96	100.20
Oxygens	8	3		12.5		22	8			
Si	2.909	–	1.002	2.994	3.001	4.779	2.444	2.794	2.678	2.893
Ti	–	1.001	0.985	–	–	–	–	–	–	–
Al^{IV}	1.081	–	0.014	–	–	3.221	1.548	1.191	1.317	1.091
Al^{VI}	–	–	–	2.947	2.913	3.955	–	–	–	–
Fe^{+3}	–	–	–	0.055	0.093	–	–	–	–	–
Fe^{+2}	–	0.979	–	–	–	0.105	–	–	–	–
Mn	–	–	–	–	–	–	–	–	–	–
Mg	–	0.019	–	–	–	–	–	–	–	–
Ca	0.125	–	1.004	2.009	1.988	1.148	0.578	0.261	0.328	0.170
Na	0.879	–	–	–	–	0.743	0.421	0.731	0.679	0.815
K	–	–	–	–	–	0.104	–	–	–	–

* FeO as Fe_2O_3

the early stage of the metamorphic history. The distribution and composition of inclusions within garnet, along with the zoning pattern of the host crystal, can be used to reconstruct the *P–T* conditions during garnet growth.

Kyanite eclogite

The inclusion assemblage albite + magnesiohornblende + clinozoisite indicates that the metamorphic growth history of the garnet started in the albite–epidote–amphibolite facies before entering the eclogite facies indicated by omphacite inclusions within the rim regions. Paragonite associated with albite (Fig. 2c) is restricted to rare inclusions trapped within garnet cores. This original paragonite might have been finally removed from the prograde assemblage according to the reaction:

Paragonite → jadeite(omphacite) + kyanite + H_2O.

The reaction occurred while garnet continued to grow, as indicated by the ubiquitous kyanite and omphacite inclusions (Fig. 2b, c). The reaction above is experimentally determined by Holland (1979) and has a shallow negative slope, which means that higher metamorphic temperatures will lower the equilibration pressures. The composition of peak-P matrix omphacite (Jd_{54}) is similar to the maximum Jd content (Jd_{55}) analyzed in omphacite inclusions, indicating that garnet growth still continued at the peak *P–T* conditions. The reaction above indicates a minimum pressure of ~2.0 GPa assuming temperatures around 600°C and H_2O activity equal to unity for a jadeite content of 55 mol%.

Common eclogite

Inclusions of glaucophane in garnet indicate that the metamorphic growth history of garnet in the common eclogite of the Kovalo area passed the epidote–blueschist facies before entering the eclogite facies manifested by omphacite inclusion within the rim regions. Inclusions of paragonite, clinozoisite and winchite (Al_2O_3 = 7.4–10 wt%, Table 5) indicate that the prograde path first passed the narrow triangular field of the albite–epidote–amphibolite facies before entering the epidote blueschist facies field (Evans 1990; see chapter about *P–T* path).

Paragonite is restricted to rare inclusions trapped within garnet. Kyanite is not present in the common eclogites, suggesting that either peak *P–T* conditions did not exceed the paragonite stability field or matrix paragonite was totally consumed by other reactions at lower pressures—a point we have tried to resolve by drawing pseudosections (see below).

Breakdown reactions and replacement textures

Post-eclogite-facies decompression results in the destruction of the eclogitic assemblages and the formation of new phases, commonly in the form of symplectites, coronas and reaction rims. The following reaction textures have been identified in the Kechros eclogites.

1. Omphacite breaks down to intergrowths of diopside-rich clinopyroxene + plagioclase, but most commonly, it is replaced by symplectites of amphibole + plagioclase (Figs. 2c, d, 3a, b).

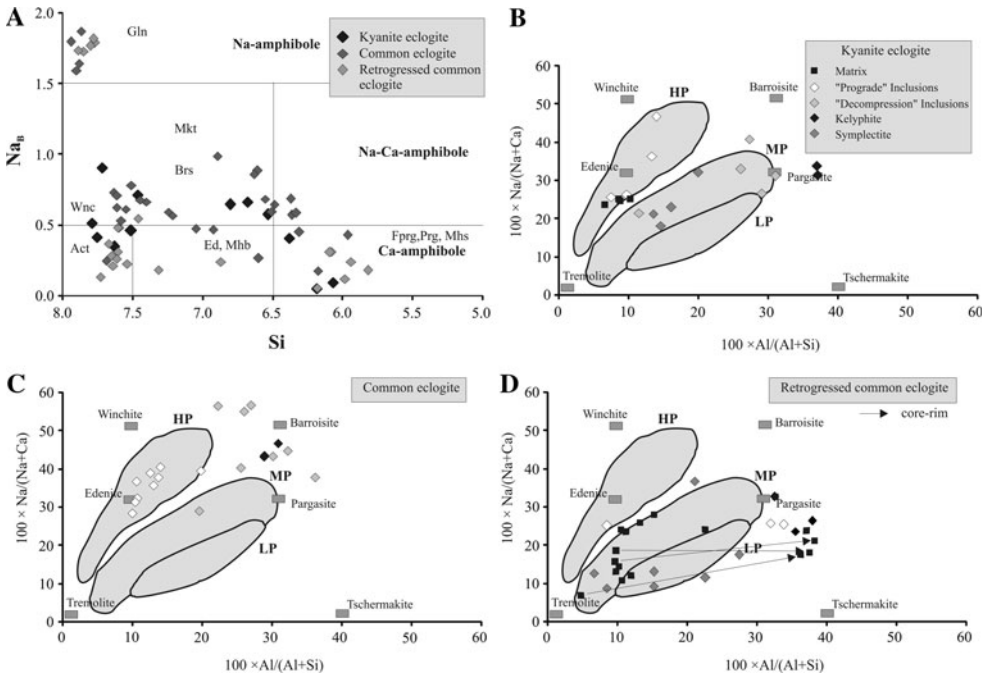

Fig. 6 Chemical composition of amphiboles in diagrams showing Na_B versus Si (**a**) and 100Na/(Na + Ca) versus 100Al/(Al + Si) (B < C < D). **b** Is from kyanite eclogite, **c** from common eclogite and **d** from retrogressed common eclogite. HP, MP and LP fields are from Laird and Albee (1988) for Ca-amphiboles from high-pressure, medium-pressure and low-pressure metabasites. *Arrows* show core to rim composition trend in zoned crystals

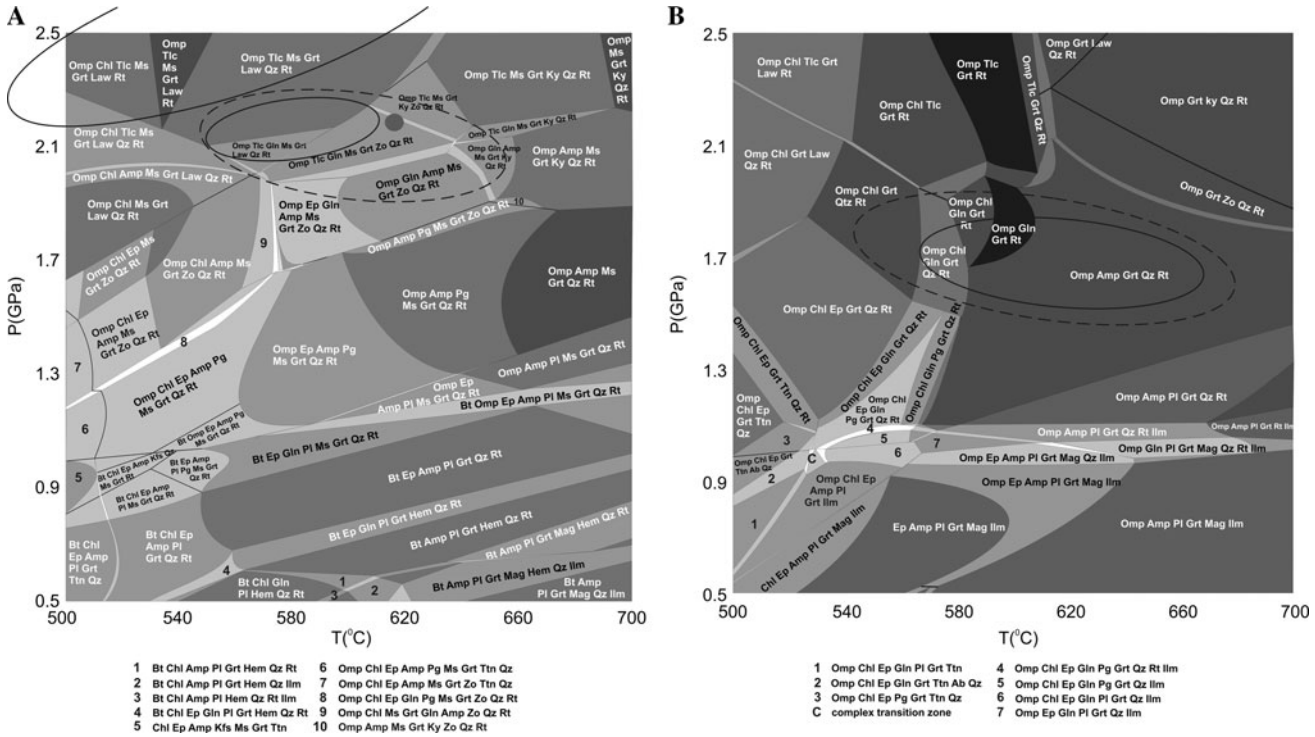

Fig. 7 *P–T*-Pseudosections of kyanite eclogite (**a**) and common eclogite (**b**). Phases modeled as solid solutions start with a *capital letter*. Some very narrow fields are just represented by *lines*. For details, see text. *Ellipses* drawn show the results of average-PT calculations (*broken lines* for quartz-absent assemblages) and are shaped according to the *P–T* correlation given in the program output. The *large gray dot* in 7A indicates *P–T* conditions calculated by classical geothermobarometry

Table 7 Garnet–clinopyroxene thermometry and garnet–clinopyroxene–phengite–kyanite thermobarometry for the eclogites from Kechros Complex

Sample	Rock type	Garnet–clinopyroxene thermometry (in °C)				
		n (number of analyzed pairs)	Ellis and Green (1979)	Powell (1985)	Krogh (1988)	Average Grt-Cpx thermometry
EK-9	Kyanite[a] eclogite*	6	637 ± 29	613 ± 29	579 ± 32	610 ± 30
	Kyanite[a] eclogite**	4	621 ± 45	598 ± 45	565 ± 49	595 ± 46
93A-8, 93A-9B, 93A-10	Common[b] eclogite*	10	514 ± 44	492 ± 44	465 ± 44	490 ± 45
93A-8, 93A-9B	Common[b] eclogite**	10	532 ± 37	508 ± 37	473 ± 36	505 ± 37

		Grt^{+}-Cpx^{++}-Ph^{+++}-Ky-SiO_2 thermobarometry (P in GPa and T in °C)					
		Grt-Ph-Ky-Qz		Grt-Ph-Cpx		Intersection	
EK-9	Kyanite eclogite	23.84	594	21.31	584	**2.20**	**615**

* Inclusion cpx, ** Matrix cpx

[+] Analysis 57, Table 2

[++] Analysis 10/M, Table 3

[+++] Analysis 13, Table 5

[a] Calculated for 2.0 GPa

[b] Calculated for 1.7 GPa

2. Garnets are replaced by kelyphitic high-Al Ca-amphibole (and plagioclase) as reaction product between garnet and omphacite (Fig. 2a, b, i) and between garnet and Na-rich tremolite (Fig. 3d).
3. Zoisite + margarite (probably formed in an early stage of decompression in the retrogressed common eclogite KO-6) + low-Al Ca-amphibole react to An-rich plagioclase and high-Al Ca-amphibole.
4. Matrix rutile is replaced by both ilmenite (Ilm-2) and titanite (Ttn-2) (Fig. 3h) during decompression, and all three phases are included in growing Ca-amphibole that shows compositional zoning with increasing Al_2O_3 content toward the rim (Fig. 6d).

During decompression, omphacitic clinopyroxene decomposes according to the reaction:

$$\text{Omphacite} + SiO_2 \rightarrow \text{less sodic clinopyroxene} + \text{plagioclase}.$$

The jadeite component in clinopyroxene ranges from Jd_6 to Jd_{14} and the anorthite component in associated symplectitic plagioclase from An_2 to An_{13}. Replacement of omphacite by symplectites of hornblende + plagioclase requires participation of H_2O and additional mineral phases in the reaction. The compositions of symplectitic amphiboles plot in the fields of LP, MP and between MP and HP (Laird and Albee 1981) (Fig. 6b, c, d). The An content in symplectitic plagioclase associated with amphibole ranges from 13 to 33%.Kelyphitic rims of amphibole and plagioclase around garnet are formed where garnet is in contact with matrix omphacite or with matrix Na-rich tremolite (Figs. 2a, i, 3c). In associated plagioclase, the anorthite component varies from An_{28} to An_{33}.Formation of plagioclase ($An_{50–58}$) and tschermakitic hornblende replacing zoisite, margarite and Na-rich tremolite in retrogressed common eclogites from Kovalo suggests that the reaction:

$$\text{Zoisite} + \text{margarite} + \text{tremolite} \rightarrow \text{anorthite} + \text{tschermakite} + H_2O,$$

occurred during decompression.

P–T estimates

Estimation of peak conditions

Three methods have been used to constrain *P–T* conditions of the major equilibration stages of the three rock types described: single, experimentally calibrated equilibria that are partly compiled in a spreadsheet program by Ravna and Terry (2004), the "average *P–T*" method of the software THERMOCALC, which uses a full set of independent reactions based on an internally consistent dataset, and *P–T* pseudosections based on the same dataset but computed with the software PERPLE_X (Fig. 7a, b).

In kyanite eclogite, the maximum *P–T* conditions were estimated quantitatively by applying the garnet–omphacite–phengite–kyanite–quartz thermobarometer of Ravna and Terry (2004) and using matrix phengite, omphacite and garnet compositions (Table 7). Pressures of 2.2 GPa and temperatures of 615°C are estimated (Table 7). The above pressure is only 0.2 GPa higher than the minimum pressure obtained from paragonite decomposition to clinopyroxene (Jd_{55}) and kyanite in the presence of pure H_2O fluid.

We have also applied the garnet clinopyroxene Fe–Mg exchange thermometer to garnet rim and adjacent matrix omphacite with the maximum jadeite component (Jd_{50}–Jd_{54}) as well as garnet and clinopyroxene inclusions with the most jadeite-rich compositions (Jd_{50}–Jd_{55}) in order to get a peak temperature estimate. Calculated temperatures are in the range of 610 ± 30°C for the garnet–clinopyroxene inclusions and 595 ± 46°C for the garnet rim-matrix omphacite pairs for pressure of 2.0 GPa. Mean values obtained from the garnet–clinopyroxene inclusion pairs show no significant deviation from the temperature obtained from the garnet–clinopyroxene–phengite–kyanite–quartz thermobarometer (Table 7).

The average *P–T* results for the kyanite eclogite (using garnet (57), omphacite (10) and phengite (13) from Tables 3, 4 and 6) are 562 ± 82°C and 2.51 ± 0.36 GPa, with a "sigfit" value of 0.99, significantly below the cutoff value of 1.96 (indicating that the χ^2 test for 95% confidence has been passed; sigfit is the scatter of the residuals (the observed minus the calculated values) of enthalpies and activities normalized by their uncertainties—see Powell and Holland 1994 for more details). No end-members had to be excluded, which corroborated that the compositions used were in fact in equilibrium with each other at one point in time. If one adds the composition of an amphibole (59 in Table 5) to the set, which has most likely been in equilibrium with the rest of the assemblage, the result does not immediately fall within the confidence interval but requires omission of the glaucophane and the acmite end-member from calculation before a reasonable value is attained, and the corresponding *P–T* conditions are significantly different than without amphibole: 582 ± 32°C and 2.17 ± 0.11 GPa. For quartz-absent conditions, this result would shift insignificantly to 600 ± 55°C and 2.11 ± 0.18 GPa. This indicates that, if amphibole was present at peak condition, its composition was sufficiently altered later to no longer fully reflect these conditions. The omitted end-members suggest sodium and ferric iron to be critically altered or imprecisely determined by the recalculation procedure (Fe^{3+}), which is not an unreasonable assumption.

In the common eclogites, a quantitative estimate of the maximum pressure is not possible by conventional geothermobarometry due to the lack of an appropriate barometer in the peak metamorphic assemblage.

The average *P–T* method can be used only if amphibole presence is assumed, otherwise there would be an insufficiently large set of independent reactions. The conditions obtained in this case (using garnet 45, omphacite 15 and amphibole 65 from Tables 3, 4 and 5) are 619 ± 53°C and 1.69 ± 0.17 GPa for the quartz-present and 612 ± 71°C and 1.71 ± 0.23 GPa for the quartz-absent case. In these cases, grossular activity needed to be shifted beyond its uncertainty limit and had to be omitted to get results within the confidence level required, which indicates that the most Ca-rich (higher-P) composition of garnet was no longer in equilibrium at the *P–T* conditions thus found.

In order to get some better constraints on the prograde path and a better idea about amphibole stability at peak

conditions, *P–T* pseudosections were computed for the kyanite eclogite and common eclogite bulk compositions (Table 1; Fig. 7a, b for used bulk compositions).

This approach is not as straightforward as it may seem at first glance because assumptions about an unknown composition parameter—the amount of ferric iron in the sample—need to be made (we chose 10% of total iron to be ferric), and several strong dependencies of results on the solid solution models turned up—specifically for that of amphibole. We did calculations in the system MnNCFMASHTO, with additional K for the kyanite eclogite (K content of the common eclogite is negligible and no K-bearing phase was observed in the rock). Mn was (absolutely) necessary to include, despite low values in the bulk rock composition, as otherwise garnet would not have been stable below 580°C and could not have recorded the earlier prograde history with inclusions of albite and paragonite in the core, as documented in the thin sections. Even though solid solution models of comparable complexity were chosen—in essence the models used successfully by Wei et al. (2003)—the most recent (and most complex) amphibole model by Diener et al. (2007) resulted in clinopyroxene stability down to unreasonably low pressures and temperatures, at the expense of plagioclase. The older amphibole model by Dale et al. (2005) restricts clinopyroxene stability to reasonable *P–T* ranges and predicts plagioclase correctly for the kyanite eclogite composition, but not for the common eclogite, where it also has been found as inclusions in garnet cores. A still older and simpler amphibole model (called GlTrTsPg in the PERPLE_X software, with interaction parameters taken from White et al. 2003 and Wei et al. 2003) predicts reasonable ranges of stability for clinopyroxenes and plagioclase and was used to compute Fig. 7a, b. An inspection of the pseudosection calculated for the kyanite eclogite (Fig. 7a) shows that the peak *P–T* conditions predicted by average *P–T* (without amphibole) fall within the stability field of talc (and lawsonite!), but not kyanite. The uncertainty ellipses for the amphibole-present and amphibole-absent case hardly touch the kyanite stability range. The result of conventional thermobarometry plots somewhat closer, at the low temperature limit of the kyanite eclogite stability field. Even though all the fields shown in that *P–T* range are quartz-bearing, only the quartz-absent average *P–T* result covers the most likely peak-assemblage fields with kyanite plus talc or amphibole(s) stable, which are also close to the *P–T* values given by conventional geothermobarometry. It is unclear at this point why the average *P–T* result for amphibole-free kyanite eclogite plots in a rather unreasonable range with regard to the pseudosection. Field boundaries in pseudosections can be quite sensitive to the solution models used—more so than conventional geothermobarometry—but the lawsonite–kyanite boundary is not that sensitive in this respect. Any method of conventional geothermobarometry can, of course, produce *P–T* results that plot in fields where the geothermobarometer assemblage is metastable.

The pseudosection for the common eclogite (Fig. 7b) shows a large stability field of omphacite + garnet + amphibole + quartz + rutile, and both the results of conventional geothermobarometry and of average *P–T* plot in that field, quite close to each other. This result also corroborates that amphibole and quartz have been part of the peak metamorphic assemblage. The amount of quartz computed is low (ca. 0.25 vol% at 610°C, 1.70 GPa), which would explain why it has not been observed in thin section.

The pseudosections of both rocks show a very sharp transition from albite to paragonite stability at around 1.0 GPa. The paragonite stability field in the common eclogite is small and can be used to narrow down the prograde path.

The observation that the configuration of phase fields changes significantly with the type of amphibole model used and that more recent models are not necessarily the better ones indicates to us that the results computed do not have a level of reliability sufficient to justify more detailed work with composition isopleths. However, the analysis of amphibole compositions computed for the pseudosections shows quite generally that Na-rich tremolite is stable only near the upper pressure stability of amphibole toward talc, which is consistent with the peak *P–T* conditions determined. At lower pressures, amphibole becomes more Al rich.

Due to the uncertainties in composition (mainly Fe^{3+}) and activity-composition models (mainly amphibole, but also white mica and clinopyroxene), we consider the results of conventional geothermobarometry and of the average *P–T* method more reliable than inferences from pseudosections, at least for basaltic bulk compositions.

P–T path

The metamorphic evolution of the Kechros eclogites in the form of a *P–T* path is given in Fig. 8. Information on the early prograde stage of metamorphism is provided by the mineral inclusions in the prograde-zoned garnets.

The presence of glaucophane inclusions in garnets from the common eclogite of the Kovalo area and the absence of blue amphiboles in the kyanite eclogite from Charakoma area could be explained by different geothermal gradients during subduction for the two eclogites. However, a detailed work on metapelites that are distributed in the whole area of the Kechros Complex showed a common *P–T* path for all metapelite occurrences of the Kechros Complex and that the decompression from the maximum

pressure down to pressure of ~0.4 GPa was within the narrow chloritoid–staurolite–chlorite stability field (Mposkos 1989; Mposkos and Liati 1993).

The presence of glaucophane in the Kovalo eclogite and the absence of it from the kyanite eclogite from Charakoma area may be attributed to the bulk rock compositions of the two eclogite types. The Kovalo eclogite is richer in iron than the kyanite eclogite. The higher iron content (Fe^{2+} as well as Fe^{3+}) enlarges the *P–T* field of the epidote–blueschist facies and shifts the boundary between epidote–blueschist and epidote–amphibolite facies to higher temperatures and lower pressures (Evans 1990; Fig. 8). Considering a common geothermal gradient for the metamorphic evolution of both eclogite types in the Kechros Complex, the absence of Na-amphibole from kyanite eclogite and the presence of glaucophane in common eclogite indicate that the prograde path passed within the overlapping transitional field of the epidote–blueschist and albite–epidote–amphibolite facies before entering the eclogite facies (Fig. 8, points B, C on the *P–T* loop). For the common eclogite, point A is constrained by the presence of albite, paragonite and tremolite inclusions in garnet cores, suggesting that the *P–T* path first crossed the small triangular field of the albite–epidote–amphibolite facies before it crossed the epidote blueschist facies.

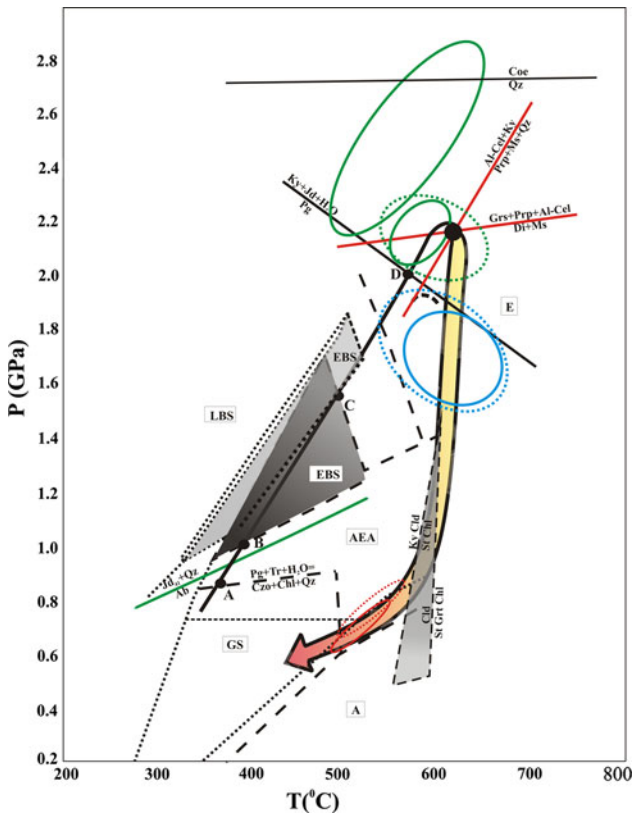

Fig. 8 *P–T* path for the eclogites of the Kechros Complex in East Rhodope. The points *A*, *B*, *C*, *D* on the *P–T* loop are constrained by textural relationships and mineral composition (see text). The peak conditions for the kyanite eclogite are obtained using garnet–omphacite–phengite geothermobarometry and average *P–T* estimates. The metamorphic facies field boundaries are after Evans (1990). *Gs* greenschist, *AEA* albite–epidote amphibolite, *EBS* epidote–blueschist, *LBS* lawsonite–blueschist, *A* amphibolite, *E* eclogite. The reaction curves are calculated with both the software THERMOCALC and the TWEEQU (windows version 2.34 Berman 2007; Berman 1991; updated database of Berman 1988; Berman and Aranovich 1996) using analyzed mineral compositions given in Tables 3, 4, 5 and 6. *Green ellipses* refer to the peak *P–T* conditions of kyanite eclogites. *Blue ellipses* refer to the peak *P–T* conditions of the common eclogites. *Red ellipses* refer to the retrograde *P–T* conditions of the retrogressed eclogites. *Ellipses* displayed by continuous lines refer to quartz-present, whereas those represented with *dotted lines* for quartz-absent conditions. The Cld + St + Chl stability field for metapelites is from Spear (1993). The reaction Pg = Ky + Jd + H_2O is from Holland (1979)

Textures and mineral compositions in the retrogressed eclogite already indicate that the degree (volume) of equilibration is quite variable, and thermobarometric results confirm this. Only a few of the local assemblages used gave reliable results (*sigfit* value below confidence limit). *P–T* conditions of 520 ± 33°C and 0.71 ± 0.1GPa were calculated for the quartz-present case and 534 ± 36°C, 0.77 ± 0.11 GPa for the quartz-absent case from the assemblage garnet (12n-2r), epidote (Ep-86), amphibole (47), plagioclase (Pl-38) of sample KO-6 (see tables).

These results suggest that much of the decompression path was nearly isothermal and crossed the chloritoid–staurolite–chlorite stability field (Fig. 8), as confirmed by the coexistence of Cld + St + Chl in the associated metapelites.

The presence of late andalusite in the high-Al metapelites of the Kechros Complex (Mposkos 1989) suggests further exhumation and cooling within the andalusite field.

The Ca-amphibole inclusions in the garnet of both eclogite types are characterized by high contents of Na_{M4} and Al^{VI} (Table 4; Fig. 6b, c) which reflect the formation at high pressures (Laird and Albee 1981).

In the kyanite eclogite, paragonite, trapped as inclusion in garnet, was succeeded by the high-pressure assemblage omphacite + kyanite (Fig. 8, D on the *P–T* loop). A minimum pressure of ~2.0 GPa is indicated by the experimental data of Holland (1979) based on the equilibrium paragonite → omphacite (jd_{55}) + kyanite + quartz, for a temperature of ~580°C. Peak *P–T* conditions are constrained at 2.2 GPa and 615°C using garnet–omphacite–phengite–kyanite–quartz geothermobarometry. However, the pseudosection shows that kyanite can also grow by other reactions, and at present, there is no additional evidence from thin sections to constrain the actual reactions forming kyanite and leading to the peak assemblage.

In the common eclogite, the only viable *P–T* constraints come from average *P–T* results (ellipse in Fig. 8), but these also indicate that peak pressures are not recorded in this type of eclogite.

The Kechros complex in the context of the regional tectonometamorphic evolution

The RD provides the opportunity for studying the complex tectonic history of a convergent plate margin during subduction and subsequent continental collision. It is important to stress that the overall history of high-P metamorphism in the RD extends over a prolonged period of time of perhaps more than 130 Ma (from ca. 180–45 Ma). However, the individual tectonic units of the RD record separate histories of HP metamorphism with quite different *P–T* conditions. Maximum *P–T* conditions and the *P–T* path of the Kechros Complex are distinct from the other under- and overlying tectonic units.

In the following, we first discuss the constraints for the formation of the Kechros Complex itself and after that the tectonic relationships of the Kechros Complex with the other HP tectonometamorphic complexes of the RD.

Tectonic constraints from the *P–T* path and lithologies of the Kechros complex

The Kechros eclogites reflect the physical conditions attained during the Alpine orogeny, as the protolith of the kyanite eclogite is a Permian gabbro that intruded the Carboniferous magmatic protolith of the orthogneiss in a continental rifting environment (Liati 2005; Liati and Fanning 2005; Baziotis and Mposkos 2010). The tectonic development of the eclogites is reflected by a clockwise *P–T* path. The prograde part of the path reflects the subduction of the Apulia continental crust (a promontory of the Africa continent), under the southern margin of the European continent, following subduction and final closure of the Axios/Vardar ocean in late Cretaceous-early Tertiary (Ricou et al. 1998; Okay and Tüysüz 1999; Mposkos and Krohe 2000; Bröcker and Pidgeon 2007 and references therein) (Fig. 9). Evidence for subduction of oceanic lithosphere along the continental margin is provided by the Kovalo eclogites and the retrogressed eclogites, which are of oceanic origin (Baziotis and Mposkos 2010), and by the associated ultramafics. The ultramafic rocks are antigorite serpentinites and contain boulders of retrogressed eclogites (this work), dykes of meta-rodingites, amphibolites and metatrondhjemites (Mposkos et al. 1997; Iliadis 2006). The mineral assemblage in the dyke amphibolites is hornblende ± clinopyroxene ± garnet + clinozoisite + albite + rutile ± titanite. The composition of hornblende shows high Na_B and Al^{VI} indicating amphibole formation at moderately high pressure (Laird and Albee 1981; Mposkos 1989; Mposkos et al. 1997). Diopside–albite symplectites and hornblende–plagioclase symplectites suggest the presence of former Na-rich clinopyroxene. In a metatrondhjemite with the mineral assemblage Ab + Pl + Bt + Pg + Na-Mrg, relict omphacite (Jd_{55}) is preserved as inclusion in albite. Most of this omphacite is decomposed to diopside (Jd_{19}) + hornblende + albite (Mposkos in preparation). The geochemical characteristics of the Kovalo eclogite and those of the amphibolitized dykes indicate ocean ridge environment for their gabbroic/basaltic protoliths (Baziotis and Mposkos 2010). All these

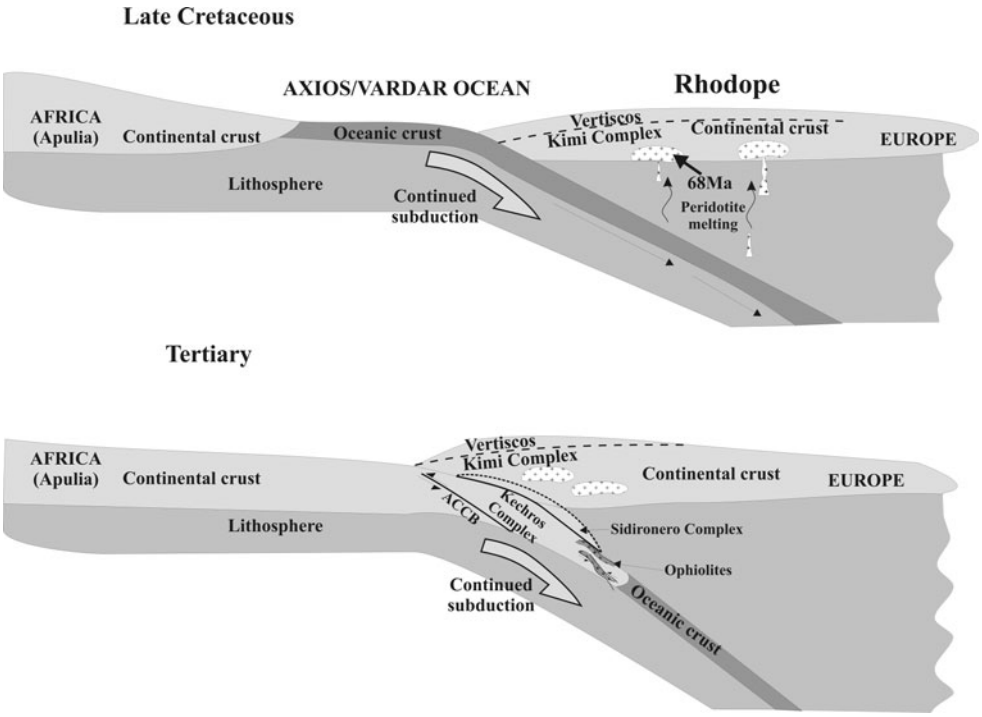

Fig. 9 Geodynamic scenario for the eclogite-facies metamorphism in the Kechros Complex from East Rhodope. The 68-Ma age of the granitoid intrusion is from Marchev et al. (2006)

features suggest that ophiolite remnants are involved in the subduction and final architecture of the Kechros Complex.

Continued convergence led to the formation of eclogite-facies assemblages in the oceanic as well as in the continental crust lithologies. Orthogneisses with Carboniferous magmatic protoliths (Liati 2005; Cornelius 2008) contain phengites with up to 3.5 Si a.p.f.u. (Mposkos 1989), indicating the involvement of continental crust in the subduction/collision process.

Geochronological data for the eclogite stage in the Kechros Complex are not yet available. The 255-Ma age of the gabbroic protolith of the kyanite eclogite (Liati 2005) indicates only Alpine HP metamorphism. A Rb–Sr white K-mica age of 37 Ma (sieve fraction > 500 μm) from a mylonitic orthogneiss is interpreted as a minimum age of the Alpine HP metamorphism (Wawrzenitz and Mposkos 1997). Ar–Ar dating of white K-mica from mylonitic orthogneisses yielded cooling ages between 36 and 41 Ma (Lips et al. 2000). Intrusion of granitoids with Rb–Sr biotite cooling ages of 32–30 Ma (Del Moro et al. 1988) indicates that the Kechros Complex was not exposed to the surface at least until the middle Oligocene.

Relationships of the Kechros complex with the other HP tectonic complexes

Ultrahigh-pressure phases like coesite and microdiamond reported from the overlying Kimi Complex (Mposkos and Kostopoulos 2001; Perraki et al. 2004, 2006; Mposkos and Krohe 2006) have not been found in the Kechros eclogites. The HP/UHP metamorphism in the Kimi Complex (Fig. 1) occurred in the early Jurassic (Bauer et al. 2007; Hoinkes et al. 2008). The Kimi Complex shows a prolonged exhumation history lasting more than 100 Ma with final exhumation to the surface between Paleocene and middle Eocene (Mposkos and Krohe 2000, 2006; Bauer et al. 2007). Minimum pressure of 2.3 GPa and temperatures of 800°C for the HP stage and 1.55–1.75 GPa and 820°C for the following granulite facies overprinting are reported from partially amphibolitized eclogites (Krenn et al. 2010; Bauer et al. 2007; Mposkos and Perdikatsis 1987).

Blueschist and eclogite-facies metamorphic rocks are reported from the southern part of East Thrace and the Biga peninsula of Turkey (Topuz et al. 2008; Okay and Satir 2000; Fig. 1 insert). Both areas lie to the SE of the Circum Rhodope Belt, which lies tectonically on top of the Kimi Complex of East Rhodope (Fig. 1). The blueschist facies tectonic sliver from East Thrace comprises serpentinites, metadiabases, blueschists, marbles and metacherts, metamorphosed at *P–T* conditions of 270–350°C and 0.65–0.80 GPa. In the Biga peninsula, the HP unit comprises quartz-mica schists with minor calc-schists, marble, quartzite and metabasite metamorphosed at *P–T* conditions of 510°C and 1.1 GPa minimum pressure. Timing of the blueschist facies metamorphism is constrained to c. 86 ± 1.5 Ma in East Thrace and 65–69 ± 1 Ma of the eclogite facies in the Biga peninsula by Rb–Sr phengite-whole rock dating (Topuz et al. 2008; Okay and Satir 2000). Pre-Alpine lithologies are not involved in both high-pressure units.

The Circum Rhodope Belt comprises mainly greenschist facies rocks with local serpentinite and metagabbro (Magganas 2002; Bonev and Stampfli 2003, 2008) with late Jurassic ^{40}Ar-^{39}Ar ages (Bonev et al. 2008). Blueschist facies assemblages have been reported from the western Circum Rhodope Belt (Michard et al. 1994).

All the above HP metamorphic complexes, the Kimi Complex in East Rhodope, the Circum Rhodope Belt and the HP rocks from East Thrace and Biga peninsula, are transgressively covered by Middle (Bartonian in East Thrace) to Upper Eocene sediments (Papadopoulos 1980; Topuz et al. 2008; Okay and Satir 2000, Okay et al. 2010) having thus been exhumed to the surface clearly earlier than the Kechros Complex.

In Western and Central Rhodope, the equivalent of the Kechros Complex is the Albite-Gneiss Series sandwiched between the overlying Sidironero Complex and the underlying Pangaeon Complex within the Nestos Shear Zone. Mposkos et al. (2010) consider the lithologies of the Albite-Gneiss Series to be a part of the Pangaeon Complex that overthrusted the marbles of the Pangaeon Complex along the Nestos Shear Zone. The emplacement of the Sidironero Complex on the Pangaeon Complex along the Nestos Shear Zone is of Paleogene age, i.e., between ca. 55–56 Ma and 32 Ma (Jahn-Awe et al. 2010). In the area between Xanthi and Komotini town, the west Kardamos detachment separates the Albite–Gneiss Series from the overlying Kimi Complex (Mposkos and Krohe 2000; Krohe and Mposkos 2002) (Fig. 1). Up to now, no eclogites were found in the Albite-Gneiss Series. The PT conditions of the HP metamorphism are constrained from the mineral assemblages in orthogneisses and metapelites at ca. 1.2 GPa and 490°C in the southwestern part of the Albite-Gneiss Series (about 40 km to the WNW of Xanthi) and ≈1.3–1.5 and ≈550°C in the area west of Komotini (western Kardamos Complex according to Mposkos and Krohe 2000). The increase in pressure from 1.2 GPa in the western part of the Albite-Gneiss Series to 1.3–1.5 GPa in the eastern part and to 2.2 GPa in the Kechros Complex indicates a direction of subduction from WSW to ENE.

In the Sidironero Complex, two Alpine HP events are reported: an early to middle Jurassic HP(UHP) event and an Eocene (52–42 Ma) one (Liati and Gebauer 1999; Liati 2005; Mposkos and Kostopoulos 2001; Reischmann and Kostopoulos 2002; Perraki et al. 2004, 2006; Hoinkes et al. 2008; Krenn et al. 2010). Mposkos et al. (2010) consider

the Sidironero Complex as a slice of the overlying Kimi Complex involved in the Eocene subduction/collision through a tectonic erosion mechanism. The Albite-Gneiss Series underwent only one Alpine, probably the Eocene HP metamorphism. ^{40}Ar-^{39}Ar white K-mica dating of mylonitic phengitic orthogneisses with Carboniferous magmatic protoliths (Turpaud and Reischmann 2010) yielded cooling ages around 36 Ma (Lips et al. 2000).

Geochronological data from HP metamorphic rocks of the Kimi Complex in Rhodope, the Circum Rhodope Belt, the East Thrace blueschists, the Biga peninsula, the Sidironero Complex in Central Rhodope and from the Kechros Complex in East Rhodope demonstrate that active subduction (and substantial accretionary crustal growth) started in the Jurassic in the Kimi Complex and in the Circum Rhodope Belt (Bauer et al. 2007; Liati 2005; Bonev et al. 2008) and continued during late Cretaceous and early Tertiary time. The *P–T* conditions of these metamorphic areas are, however, highly different: ultra-high-pressure conditions in the uppermost Kimi Complex in the Rhodope Domain, greenschist- to local blueschist-facies conditions in the Circum Rhodope Belt, blueschist/eclogite facies in the southern part of East Thrace and the Biga peninsula and eclogite facies in the Kechros Complex, which is the lowermost tectonic unit in the East Rhodope core complex.

Eocene blueschist- to eclogite-facies metamorphism is well documented in the Attic-Cycladic Crystalline Belt (ACCB, Fig. 1 insert, cf. Matthews and Schliestedt 1984; Bröcker et al. 1993; Trotet et al. 2001 and references therein). The ACCB consists of two major structural units that are separated by low-angle normal faults (e.g., Lister et al. 1984; Dürr et al. 1978; Okrusch and Bröcker 1990; Avigad et al. 1997; Jolivet et al. 2003). The lower tectonic unit of the ACCB comprises a pre-Alpine basement including Carboniferous granitoid protoliths, Mesozoic volcanosedimentary series and dismembered ophiolites, lithologies that are similar to those of the Kechros Complex in East Rhodope. The lower tectonic unit of the ACCB underwent Eocene (55–40 Ma) blueschist- to eclogite-facies metamorphism with *P–T* conditions of 1.2–2 GPa and ~450–550°C and an Oligocene (35–25 Ma) greenschist- to amphibolite-facies overprint (e.g., Matthews and Schliestedt 1984; Bröcker et al. 1993; Trotet et al. 2001 and references therein). The upper tectonic unit of the ACCB comprises a heterogeneous sequence of unmetamorphosed Permian to Mesozoic sediments, ophiolites, greenschist facies rocks of Cretaceous age as well as late Cretaceous (80–70 Ma) MP/HT rocks and granitoids (e.g., Reinecke et al. 1982; Patzak et al. 1994; Bröcker and Franz 2006). that were not affected by the Tertiary HP metamorphism (Dürr 1986). These rocks are exposed only in small areas and may be correlated with the uppermost tectonic complexes of the Rhodope, including the Kimi Complex of East Rhodope recording late Cretaceous MP amphibolite facies metamorphism (78–71 Ma) and granitoid magmatism (80–69 Ma) (Liati et al. 2002; Bauer et al. 2007; Peytcheva et al. 1999; Marchev et al. 2005; Bonev et al. 2010). However, despite these similarities, a direct correlation between the Kechros Complex from East Rhodope and the Cyclades blueschist/eclogite unit is not straightforward. This is because extensional tectonics, which started in the Oligocene in the Rhodope area (Krohe and Mposkos 2002) and continued until present in the South Aegean region, disrupted the original tectonic relationships among the different HP metamorphic units at different scales. No metamorphic rocks are exposed on the islands of Limnos and Agios Efstratios, which lie between the Rhodope and the Cyclades. They are covered by late Eocene and post-Eocene sediments and volcanics.

In their schematic tectonic model for the evolution of the Rhodope Domain, Jahn-Awe et al. (2010) propose the following:

1. a SW subduction of the upper tectonic complexes (Vertiscos and Kimi Complexes) in the Jurassic;
2. a late Cretaceous switch of subduction polarity to the NE, such that in the Tertiary, the Rhodope is characterized by SW thrusting of the tectonic units above the Apulian plate;
3. a separate evolution of the Kimi complex and the Sidironero complex (Rhodope Terrane in their figure 17) in the Jurassic.

However, there are no structural and petrological evidences from the Kimi and Vertiscos Complexes that would support a SW subduction. Also, these two complexes underwent quite different *P–T* histories, suggesting separate tectonometamorphic evolutions. In the Vertiskos Complex, the grade of the Jurassic to early Cretaceous medium-pressure metamorphism increases from garnet–chloritoid zone in SW to staurolite–kyanite grade in the NE (Mposkos unpublished data). Instead, the Jurassic metamorphic PT conditions and the Jurassic ages in the Kimi and Sidironero Complexes are very similar (Liati 2005; Bauer et al. 2007; Hoinkes et al. 2008; Krenn et al. 2010).

According to Jahn-Awe et al. (2010), the Pangaeon Complex represents the margin of the Apulian carbonate platform and is in a tectonic position equivalent to the Olympos window, which itself is in a structural position below the HP metamorphic rocks of ACCB. This correlation is in agreement with the interpretation of the Kechros Complex having a comparable tectonometamorphic evolution to the ACCB.

Conclusions

Regional high-pressure metamorphism with peak conditions of at least 585 ± 32°C and 2.17 ± 0.11 GPa in kyanite eclogite and 619 ± 53°C and 1.69 ± 0.17 GPa in "common" eclogite and retrograde conditions of 534 ± 36°C and 0.77 ± 0.11 GPa have been derived for the Kechros Complex—a tectonic unit situated below the ultrahigh-pressure Kimi and Sidironero Complexes of the Greek Rhodope. The exact role of this complex and its tectonic history will become clearer as soon as geochronological data become available for the various stages. A high-pressure stage significantly younger than UHP metamorphism in the Kimi-Complex (≥180 Ma), i.e., in the Eocene, similar to that in the Sidironero Complex and the Attic-Cycladic Crystalline Belt is considered likely at this stage.

Acknowledgments I. B. and E. M. were financially supported by the Special Research project "PEBE 2008" funded by National Technical University of Athens. Alexander Krohe is thanked for stimulating discussions and his assistance in formulating our geotectonic views. Careful and constructive reviews by Aral Okay and an anonymous reviewer have helped to improve the manuscript. We want to express our sincere thanks to Wolf-Christian Dullo and Ingo Braun for their editorial handling.

References

Avigad D, Garfunkel Z, Jolivet L, Azanon JM (1997) Back arc extension and denudation of Mediterranean eclogites. Tectonics 16:924–941

Bauer C, Rubatto D, Krenn K, Proyer A, Hoinkes G (2007) A zircon study from the Rhodope metamorphic complex, N-Greece: time record of a multistage evolution. Lithos 99:207–228

Baziotis I, Mposkos E (2010) Geochemistry and tectonic setting of eclogite protoliths from Kechros Complex in East Rhodope (N.E. Greece). In: Proceedings of the 12th international congress, geological society of Greece, XLIII(5), pp 2522–2531

Berman RG (1988) Internally-consistent thermodynamic data for stoichiometric minerals in the system Na_2O–K_2O–CaO–MgO–FeO–Fe_2O_3–Al_2O_3–SiO_2–TiO_2–H_2O–CO_2. J Petrol 29:445–522

Berman RG (1991) Thermobarometry using multiequilibrium calculations: a new technique with petrologic applications. Can Mineral 29:833–855

Berman RG (2007) WinTWQ (version 2.3) A software package for performing internally-consistent thermobarometric calculations. Geological survey of Canada, open file 5462 (revised)

Berman RG, Aranovich LY (1996) Optimized standard state and solution properties of minerals. Contrib Mineral Petrol 126:1–24

Bonev N, Stampfli G (2003) New structural and petrologic data on Mesozoic schists in the Rhodope (Bulgaria): Geodynamic implications. C R Geosci 335:691–699

Bonev N, Stampfli G (2008) Petrology, geochemistry and geodynamic implications of Jurassic island arc magmatism as revealed by mafic volcanic rocks in the Mesozoic low-grade sequence, eastern Rhodope, Bulgaria. Lithos 100:210–233

Bonev N, Burg JP, Ivanov Z (2006) Mesozoic-Tertiary structural evolution of an extensional gneiss dome the Kesebir-Kardamos dome, eastern Rhodope (Bulgaria-Greece). Int J Earth Sci 95:318–340

Bonev N, Spikings R, Moritz R, Marchev P (2008) Structural and 40Ar/39Ar age constraints on the Kulidjik nappe: a record of an early Alpine thrust tectonics in the northeastern Rhodope Massif. Symposium on the geology of the Aegean, University of Texas at Austin, Bulgaria, 28–30 April

Bonev N, Spikings R, Moritz R, Marchev P (2010) The effect of early Alpine thrusting in late-stage extensional tectonics: evidence from the Kulidzhik nappe and the Pelevun extensional allochthon in the Rhodope Massif, Bulgaria. Tectonophysics 488:256–281

Bosse V, Boulvais P, Gautier P, Tiepolo M, Ruffet G, Devidal JL, Cherneva Z, Gerdjikov I, Paquette JL (2009) Fluid-induced disturbance of the monazite Th–Pb chronometer: in situ dating and element mapping in pegmatites from the Rhodope (Greece, Bulgaria). Chem Geol 261(3–4):286–302

Bröcker M, Franz L (2006) Dating metamorphism and tectonic juxtaposition on Andros Island (Cyclades, Greece): results of a Rb–Sr study. Geol Mag 143:609–620

Bröcker M, Pidgeon R (2007) Protolith ages of meta-igneous and metatuffaceous rocks from the cycladic blueschist unit, Greece: results of a reconnaissance U–Pb zircon study. J Geol 115:83–98

Bröcker M, Kreuzer H, Matthews A, Okrusch M (1993) 40Ar/39Ar and oxygen isotope studies of polymetamorphism from Tinos Island, cycladic blueschist belt. J Met Geol 11:223–240

Burg JP, Ricou LE, Ivanov Z, Godfriaux I, Dimov D, Klain L (1996) Syn-metamorphic nappe complex in the Rhodope Massif: structure and kinematics. Terra Nova 8:6–15

Cherneva Z, Georgieva M (2005) Metamorphozed Hercynian granitoids in the Alpine structures of the Central Rhodope, Bulgaria: geotectonic position and geochemistry. Lithos 82:149–168

Cornelius NK (2008) UHP metamorphic rocks of the Eastern Rhodope Massif, NE Greece: new constraints from petrology, geochemistry and zircon ages. PhD thesis, Johannes-Gutenberg Universität, Mainz

Dale J, Powell R, White L, Elmer FL, Holland TJB (2005) A thermodynamic model of Ca–Na–amphiboles in Na_2O–CaO–FeO–MgO–Al_2O_3–SiO_2–H_2O–O for petrological calculations. J Metamorph Geol 23:771–791

Del Moro A, Innocenti F, Kyriakopoulos C, Manetti P, Papadopoulos P (1988) Tertiary granitoids from Thrace (Northern Greece): Sr isotopic and petrochemical data. Neues Jahrbuch für Mineralogie Abhandlungen 159:113–135

Diener JFA, Powell R, White RW, Holland TJB (2007) A new thermodynamic model for clino- and orthoamphiboles in the system Na_2O–CaO–FeO–MgO–Al_2O_3–SiO_2–H_2O–O. J Metamorph Geol 25:631–656

Dürr S (1986) Das Attisch-Kykladische Kristallin, Ostagaische Inseln und Gebirgsverbindungen im Agais-Bereich. In: Jacobshagen V (ed) Geologie von Griechenland. Bornträger, Berlin, pp 116–148

Dürr S, Altherr R, Keller J, Okrusch M, Seidel E (1978) The Median Aegean Crystalline Belt: stratigraphy, structure, metamorphism, magmatism. In: Closs H, Roeder DH, Schmidt K (eds) Alps, Apennines, Hellenides. IUGS report no. 38. Schweizerbart, Stuttgart, pp 455–477

Ellis DJ, Green DH (1979) An experimental study of the effect of Ca upon garnet-clinopyroxene Fe–Mg exchange equilibria. Contrib Mineral Petrol 71:13–22

Evans BW (1990) Phase relations of epidote–blueschists. Lithos 25:3–23

Franz G, Thomas S, Smith DC (1986) High-pressure phengite decomposition in the Weissenstein eclogite, Mönchberger, Gneiss Massif, Germany. Contrib Mineral Petrol 92:71–85

Hoinkes G, Krenn E, Rubatto D, Krenn K, Proyer A, Bernhard F, Bauer C (2008) Timing the Rhodope UHP-event using zircon and monazite. Paper presented at 33rd IGC Oslo, international geological congress, Oslo, Norway

Holland TJB (1979) Experimental determination of the reaction paragonite = jadeite + kyanite + H_2O, and internally consistent thermodynamic data for part of the system Na_2O–Al_2O_3–SiO_2–H_2O, with applications to eclogites and blueschists. Contrib Mineral Petrol 68:293–301

Hsü KJ, Nachev IK, Vuchev VT (1977) Geologic evolution of Bulgaria in light of plate tectonics. Tectonophysics 40:245–256

Iliadis A (2006) Study of the ultrabasic rocks of Ano Virsini (Geology–Petrology–Metallogeny). Phd Dissertation, National Technical University of Athens, pp 236 (in Greek with English abstract)

Ivanov Z, Dimov D, Sarov S (2000) Tectonic position, structure and tectonic evolution of the Rhodope massif, in structure, Alpine evolution and Mineralizations of the Central Rhodope area (South Bulgaria), In: Ivanov Z (ed) AMCD-GEODE 2000 workshop, borovets, Sofia, pp 1–20

Jahn-Awe S, Froitzheim N, Nagel TJ, Frei D, Georgiev N, Pleuger J (2010) Structural and geochronological evidence for Paleogene thrusting in the Western Rhodopes (SW Bulgaria): elements for a new tectonic model of the Rhodope Metamorphic Province. Tectonics 29: TC3008, 30 pp

Janak M, Froitzheim N, Georgiev N, Nagel TJ, Sarov S (2011) P–T evolution of kyanite eclogite from the Pirin Mountains (SW Bulgaria): implications for the Rhodope UHP Metamorphic Complex. J Metamorph Geol 29:317–332

Jolivet L, Faccenna C, Goffé B, Burov E, Agard P (2003) Subduction tectonics and exhumation of high-pressure metamorphic rocks in the Mediterranean orogens. Am J Sci 303:353–409

Kilias A, Mountrakis D (1990) Kinematics of the crystalline sequences in the western Rhodope massif. Geologica Rhodopica, 2nd Hellenic-Bulgarian symposium, Thessaloniki, vol 2, pp 100–116

Krenn K, Bauer C, Proyer A, Klötzli U, Hoinkes G (2010) Tectonometamorphic evolution of the Rhodope orogen. Tectonics 29. doi:10.1029/2009TC002513

Krogh EJ (1988) The garnet-clinopyroxene Fe–Mg geothermometer—a reinterpretation of existing experimental data. Contrib Mineral Petrol 66:75–80

Krohe A, Mposkos E (2002) Multiple generations of extensional detachments in the Rhodope Mountains (N. Greece): evidence of episodic exhumation of high-P rocks. In: Blundell DJ, Neubauer G, Von Quant A (eds) The timing and location of major ore deposits in an evolving orogen. Geol Soc Lond Special Publ 204:151–178

Laird J, Albee AL (1981) Pressure, temperature, and time indicators in mafic schists: their application to reconstructing the polymetamorphic history of Vermont. Am J Sci 281:127–175

Leake BE, Woolley AR, Arps CES, Birch WD, Gilbert MC, Grice JD, Hawthorne FC, Kato A, Kisch HJ, Krivovichev VG, Linthout K, Laird J, Mandarino JA, Maresch WV, Nickel EH, Rock NMS, Schumacher JC, Smith DC, Stephenson NCN, Ungaretti L, Whittaker EJW, Youshi G (1997) Nomenclature of amphiboles: report of the subcommittee on amphiboles of the International Mineralogical Association. Commission on new minerals and mineral names. Am Mineral 82:1019–1037

Liati A (2005) Identification of repeated Alpine (ultra) high-pressure metamorphic events by U–Pb SHRIMP geochronology and REE geochemistry of zircon: the Rhodope zone of Northern Greece. Contrib Mineral Petrol 150:608–630

Liati A, Fanning CM (2005) Eclogites and their country rock orthogneisses in East Rhodope representing Upper Permian gabbros and Upper Carboniferous granitoids: geochronological constraints. Mitt Oesterr Mineral Ges 150:88

Liati A, Gebauer D (1999) Constraining the prograde and retrograde P–T–t path of Eocene HP-rocks by SHRIMP dating of different zircon domains: inferred rates of heating, burial, cooling and exhumation for central Rhodope, northern Greece. Contrib Mineral Petrol 135:340–343

Liati A, Mposkos E (1990) Evolution of the eclogites in the Rhodope Zone of northern Greece. Lithos 25:89–99

Liati A, Gebauer D, Wysoczanski R (2002) U–Pb SHRIMP dating of zircon domains from UHP garnet-rich mafic rocks and late pegmatoids in the Rhodope zone (N Greece); evidence for Early Cretaceous crystallization and Late Cretaceous metamorphism. Chem Geol 184:281–299

Lips ALW, White SH, Wijbrans JR (2000) Middle–Late Alpine thermotectonic evolution of the southern Rhodope Massif, Greece. Geodyn Acta 13:281–292

Lister G, Banga G, Feenstra A (1984) Metamorphic core complexes of cordilleran type in the Cyclades, Aegean sea, Greece. Geology 12:221–225

Magganas AC (2002) Constraints on the petrogenesis of Evros ophiolite extrusives, NE Greece. Lithos 65:165–182

Marchev P, Kaiser-Rohrmeier M, Heinrich C, Ovtcharova M, von Quadt A, Raicheva R (2005) 2: Hydrothermal ore deposits related to post-orogenic extensional magmatism and core complex formation: the Rhodope Massif of Bulgaria and Greece. Ore Geol Rev 27:53–89

Marchev P, von Quadt A, Peycheva I, Ovtchatova M (2006) The age and origin of the Chuchuliga and Rosino granites, Eastern Rhodopes. In: Proceedings of annual conference of the Bulgaria geological society "Geosciences 2006", pp 213–216

Matthews A, Schliestedt M (1984) Evolution of the blueschist and greenschist facies rocks of Sifnos, Cyclades, Greece. Contrib Mineral Petrol 88:150–163

Michard A, Goffé B, Liati A, Mountrakis D (1994) Découverte du faciés schiste blue dans le nappes du Circum-Rhodope: un element d'une ceinture HP-BT éohellénique en Grèce septentrionale? CR Acad Sci Paris Ser II 318:1535–1542

Morimoto N (1988) Nomenclature of pyroxenes. Mineral Mag 52:535–550

Mposkos E (1989) High-pressure metamorphism in gneisses and pelitic schists in the Eat Rhodope Zone (N. Greece). Mineral Petrol 41:25–39

Mposkos E, Kostopoulos D (2001) Diamond, former coesite and supersilicic garnet in metasedimentary rocks from the Greek Rhodope: a new ultrahigh-pressure metamorphic province established. Earth Planet Sci Lett 192:497–506

Mposkos E, Krohe A (2000) Petrological and structural evolution of continental high pressure (HP) metamorphic rocks in the Alpine Rhodope domain (N. Greece). In: Proceedings of the 3rd international conference on the geology of the Eastern Mediterranean, pp 221–232

Mposkos E, Krohe A (2006) *P–T*-deformation paths of closely associated UHP (diamond-bearing) crustal and mantle rocks of the Kimi complex: implications for the tectonic history of the Rhodope Mountains, northern Greece. Can J Earth Sci 43:1755–1776

Mposkos E, Liati A (1993) Metamorphic evolution of metapelites in the high-pressure terrane of the Rhodope zone, Northern Greece. Can Min 31:401–424

Mposkos E, Perdikatsis V (1987) High-pressure metamorphism in East Rhodope Massif (Greece). Fortschr Mineral 65:140

Mposkos E, Perdikatsis V (1989) Eclogite-amphibolites in the east Rhodope massif. Geologica Rhodopica 1:160–168

Mposkos E, Wawrzenitz N (1995) Metapegmatites and pegmatites bracketing the time of HP-metamorphism in polymetamorphic rocks of the E-Rhodope: petrological and geochronological constraints. Geol Soc Greece Special Publ 2(4):602–608

Mposkos E, Orfanoudaki A, Perdikatsis V (1997) Petrological study of the amphibolite dykes in ultramafic rocks of the lower tectonic unit, from East Rhodope. Mineral Wealth 103:25–37 (in Greek with English abstract)

Mposkos E, Krohe A, Baziotis I (2010) Alpine polyphase metamorphism in metapelites from Sidironero complex (Rhodope domain, NE Greece). XIX congress of the Carpathian-Balkan Geological Association, Thessaloniki 23–26 Sept 2010

Okay AI, Satır M (2000) Upper Cretaceous eclogite-facies metamorphic rocks from the Biga Peninsula, northwest Turkey. Turkish J Earth Sci 9:47–56

Okay AI, Tüysüz O (1999) Tethyan sutures of northern Turkey. In: Durand B, Jolivet L, Horváth F, Séranne M (eds) The Mediterranean Basins: tertiary extension within the Alpine Orogen, Geol Soc Lond Special Publ 156:475–515

Okay A, Özcan E, Cavazza W, Okay N, Less G (2010) Basement types, Lower Eocene series, Upper Eocene olistostromes and the initiation of the southern Thrace basin, NW Turkey. Turkish J Earth Sci 19:1–25

Okrusch M, Bröcker M (1990) Eclogite facies rocks in the Cycladic blueschist belt, Greece: a review. Eur J Min 2:451–478

Papadopoulos P (1980) Geologic map of Greece, scale 1:50000, Sheet Feres-Peplos-Ainos. Institute of Geology and Mineral Exploration (I.G.M.E.), Athens

Patzak M, Okrusch M, Kreuzer H (1994) The Akrotiri unit on the island of Tinos, Cyclades, Greece: witness to a lost terrane of Late Cretaceous age. Neues Jahrbuch für Geologie und Paläontologie Abhandlungen 194:211–252

Perraki M, Proyer A, Mposkos E, Kaindl R, Baziotis I, Hoinkes G (2004) Micro- and nanodiamonds in garnets of metapelitic rocks from the Greek Rhodope: an in situ micro-Raman study. In: Proceedings of the 5th international symposium for Eastern Mediterranean geology, pp 1216–1219

Perraki M, Proyer A, Mposkos E, Kaindl R, Hoinkes G (2006) Raman micro-spectroscopy on diamond, graphite and other carbon polymorphs from the ultrahigh-pressure metamorphic Kimi complex of the Rhodope Metamorphic Province, NE Greece. Earth Planet Sci Lett 241:672–685

Peytcheva I, von Quadt A (1995) U–Pb zircon dating of metagranites from Byala Reka region in the east Rhodopes, Bulgaria. In: Proceedings XV congress of the Carpathian-Balkan Geological Association, Spec Publ 4:637–642, Geol Soc, Greece, Athens

Peytcheva I, Kostitsin Y, Salnikova E, von Quadt A, Kamenov B, Klain L (1999) Alpine evolution of the magmatism in the west Rhodopes: Rb–Sr and U–Pb isotope data. J Conf Abstr 4:470

Powell R (1985) Regression diagnostics and robust regression in geothermometer/geobarometer calibration: the garnet-clinopyroxene geothermometer revisited. J Met Geol 3:231–243

Powell R, Holland T (1994) Optimal geothermometry and geobarometry. Am Min 79:120–133

Ravna EJK, Terry MP (2004) Geothermobarometry of UHP and HP eclogites and schists-an evaluation of equilibria among garnet–clinopyroxene–kyanite–phengite–coesite/quartz. J Metamorph Geol 22:579–592

Reinecke Th, Altherr R, Hartung B, Hatzipanagiotou K, Kreuzer H, Harre W, Klein H, Keller J, Geenen E, Boger H (1982) Remnants of a late Cretaceous high temperature belt on the island of Anafi (Cyclades, Greece). Neues Jahrb Min Abh 145:157–182

Reischmann T, Kostopoulos D (2002) Timing of UHPM in metasediments from the Rhodope Massif, N Greece. Goldschmidt Conference Abstracts, A633

Ricou LE, Burg JP, Godfriaux I, Ivanov Z (1998) Rhodope and Vardar: the metamorphic and olistostromic paired belts related to Cretaceous subduction under Europe. Geodyn Acta 11:285–309

Spear FS (1993) Metamorphic phase equilibria and pressure–temperature–time Paths. Mineralogical Society of America, Washington, DC

Topuz G, Okay AI, Altherr R, Satir M, Schwarz WH (2008) Late cretaceous blueschist facies metamorphism in southern Thrace (Turkey) and its geodynamic implications. J Met Geol 26:895–913

Trotet F, Jolivet L, Vidal O (2001) Tectono-metamorphic evolution of Syros and Sifnos islands (Cyclades, Greece). Tectonophysics 338:179–206

Turpaud P, Reischmann T (2010) Characterisation of igneous terranes by zircon dating: implication for UHP occurrences and suture identification in the central Rhodope, northern Greece. Int J Earth Sci 99:567–591. doi:10.1007/s00531-008-0409-x

Wawrzenitz N, Mposkos E (1997) First evidence for lower Cretaceous HP/HT-metamorphism in the Eastern Rhodope, North Aegean Region, North-East Greece. Eur J Min 9:659–664

Wei CJ, Powell R, Zhang LF (2003) Eclogites from the south Tianshan, NW China: petrological characteristic and calculated mineral equilibria in the Na2O–CaO–FeO–MgO–Al_2O_3–SiO_2–H_2O system. J Met Geol 21(2):163–179

White RW, Powell R, Phillips GN (2003) A mineral equilibria study of the hydrothermal alteration in mafic greenschist facies rocks at Kalgoorlie, Western Australia. J Met Geol 21:455–468

Whitner D, Evans B (2010) Abbreviations for names of rock-forming minerals. Am Mineral 95:185–187